Contrib Mineral Petrol (1999) 136: 131–153

Antonio García-Casco · Rafael Luis Torres-Roldán

Natural metastable reactions involving garnet, staurolite and cordierite: implications for petrogenetic grids and the extensional collapse of the Betic-Rif Belt

Received: 6 August 1998 / Accepted: 9 February 1999

Abstract Medium grade metapelites of the Torrox unit (Betic-Rif Belt, S Spain) contain mineral assemblages consisting of garnet (Grt), staurolite (St), cordierite (Crd), biotite, kyanite, sillimanite, andalusite, muscovite (Ms) and quartz (Qtz) and record complex reaction processes of cordierite growth through garnet and staurolite decomposition. The reaction textures, the chemical composition of the reactant and product phases, including Fe-Mg-Mn partitioning, and the results of equilibrium thermodynamic calculations indicate that these cordierite-bearing assemblages are largely deviated from equilibrium. Furthermore, the actual cordierite-forming reactions, as estimated from the assemblage and associated textures, conflict with the predictions of thermodynamically based petrogenetic grids for the model pelite system KFMASH, either those that predict the stable coexistence of cordierite + muscovite plus garnet or staurolite or those that do not foresee a field of stability for these types of assemblages. This conflict is explained in terms of cordierite growth (at ca. 575 °C and 2.5 kbar) through metastable reactions whose operation was conditioned by the relict persistence of higher pressure phases (garnet and staurolite) and phase compositions (e.g. muscovite and biotite) after fast decompression. This interpretation militates against the existence of a wide *P-T* range of stable coexistence at low *P* of Crd + Ms + Qtz ± Grt ± St in medium grade metapelites of normal composition (i.e. poor in Zn and/or Mn). The triggering of metastable cordierite-forming reactions and the preservation of even subtle disequilibrium features associated to them indicate that the rocks underwent fast near-isothermal decompression from ca. 12 kbar down to 2–3 kbar, then rapid cooling. These inferences agree with independent evidence indicating that termination of alpine metamorphism in the western Betic-Rif Belt was related to the extensional collapse of thickened crust and that the latter had consisted of a single, continuous event.

A. García-Casco (✉) · R.L. Torres-Roldán
Departamento de Mineralogía y Petrología, Universidad de Granada, Fuentenueva s/n, E-18002 Granada, Spain; E-mail: agcasco@goliat.ugr.es

Editorial responsibility: W. Schreyer

Introduction

Most contemporary views about the orogenic evolution of the Betic-Rif Belt (S Spain and N Morocco) acknowledge the occurrence of a major Late Oligocene to Early Miocene extensional event (Torres-Roldán 1979; Platt and Vissers 1989; García-Dueñas et al. 1992; Monié et al. 1994; Docherty and Banda 1995; Vissers et al. 1995; Zeck 1996; Lonergan and White 1997; Platt et al. 1998). This notion emerged, among other sources of evidence, from studies on the evolution of metamorphism in the Alpujarride/Sebtide crustal domain of the belt. In this domain, combined thermochronological and geological constraints indicate that metamorphism came to an end about 22–18 Ma ago, and that termination of metamorphism took place through rapid cooling (as high as 250–450 °C/Ma) and uplift (in the range of several km/Ma; Zeck et al. 1989, 1992; Monié et al. 1994; Andriessen and Zeck 1996; Sosson et al. 1998; Platt et al. 1998). Further, most published *P-T* paths from Alpujarride/Sebtide sequences include a stage of near-isothermal decompression, with a pressure decrease ranging from 8 to 15 kbar (e.g. Torres-Roldán 1974, 1981; Westerhoff 1977; Couturié and Kornprobst 1977; Bakker et al. 1989; Tubía and Gil Ibarguchi 1991; García-Casco et al. 1993; García-Casco and Torres-Roldán 1996; Platt et al. 1996; Balanyá et al. 1997; Tubía et al. 1997; Azañón et al. 1998; Soto and Platt 1999), indicating that considerable uplift had already preceded final cooling. During near-isothermal decompression, incomplete reaction and disequilibrium overprinting of high-*P* assemblages by low-*P* assemblages were commonplace (García-Casco et al. 1993; García-Casco and Torres-Roldán 1996; Soto and Platt 1999), suggesting

that uplift during this stage was also very fast, and consistent with the occurrence of extensional collapse of thickened crust. Study of these disequilibrium features, in many instances well preserved after the rapid thermal relaxation in the Lower Miocene, is thus a key to understanding the late tectonic development of the Beti-Rif Belt, while providing an unusual framework to compare natural metamorphic development against the reaction path expected from theoretical models.

Generalized disequilibrium and evidence of irreversible reactions in the alpujarride rocks were first identified by Loomis (1972a, b, c, 1975a, b, 1976, 1977, 1979) in metapelites from the Casares-Los Reales unit (his "gneiss series"), located on top of the ultramafic bodies of Ronda (Fig. 1). Loomis envisaged metamorphism in this sequence as a contact aureole (a view that has kept appearing in literature reviews of metamorphism, e.g. Kerrick 1990; Pattison and Tracy 1991), and postulated that large overstepping of equilibrium boundaries in low-to-medium grade rocks had resulted from near-isobaric thermal input induced by the diapiric intrusion of the peridotite bodies. Overstepping due to decompression was recognized only in the higher grade rocks adjacent to the peridotites, that he related to fast dragging during the intrusion. Subsequent structural studies have questioned Loomis' model of peridotite intrusion and contact metamorphism (cf. Lundeen 1978; Tubía and Cuevas 1986; Van der Wal and Vissers 1993, 1996; Tubia 1994; Tubia et al. 1997), and disequilibrium metamorphic features in the Casares-Los Reales type of units are presently believed to have generally resulted from decompression, as suggested by Torres-Roldán (1981), and documented in detail by García-Casco et al. (1993) and García-Casco and Torres-Roldán (1996). Still, it is the merit of Loomis to have realized the occurrence of pervasive disequilibrium in these rocks, the interest of their study, and the usefulness of petrologic analysis in their interpretation. In their study of the Torrox metapelites (an eastern equivalent of the Casares-Los Reales sequence), García-Casco and Torres-Roldán (1996) showed that, while compositional disequilibrium and metastable persistence of high-*P* relicts almost rule out obtaining precise thermobarometric estimates in these rocks, their *P-T* evolution could generally be well constrained by comparing texturally deduced reactions and reaction history with the predictions of thermodynamically calculated petrogenetic grids. Among the complex assemblages present in most of the Torrox metapelites, there are some samples that stand out in that they contain up to 9 solid KFMASH phases, Grt + St + Ky + Fib + And + Crd + Bt + Ms + Qtz (abbreviations after Kretz, 1983), an assemblage that is likely to be among the more complex ever described in medium grade metapelites and where the relations among cordierite, garnet and staurolite (plus quartz and muscovite) are of particular interest in view of the controversial nature of Crd ± Grt ± St assemblages (see Pattison and Tracy 1991). In this paper we focus on the origin of cordierite in these rocks, and its bearing on current *P-T* grids and the development of extensional collapse of the Betic-Rif Belt.

Fig. 1 **A** Geological map of the Western Betic Cordilleras. [*1* External zones, *2* Betic Dorsal, *3* Nieves unit, *4, 5* Casares-Los Reales type of units (*4* Yunquera), including peridotite bodies (*crosses*), *6* Blanca type of units, *7* Malaguide units, *8* Early Cretaceous to Early Miocene flysch, *9* Miocene syn-tectonic deposits (type La Viñuela), *10* Neogene and Quaternary deposits (post-tectonic)]. The *box* denotes the location of the Torrox area shown in **B**. **B** Geological map of the Torrox area, with the distribution of mineral assemblages in the metapelites of the Torrox unit and the location of representative samples with cordierite-bearing assemblages. Also indicated is the location of the samples in Table 1

Geological and petrological setting

The samples come from the Torrox unit, that is located in the western-central segment of the Betic Cordillera (Fig. 1), within the Vélez Málaga-Sierra Tejeda massif. This region has been studied by Boulin (1970), Elorza et al. (1979), Elorza and García-Dueñas (1981) and Sanz de Galdeano (1989), and includes several tectonic units with metamorphic sequences of varying grade. The Torrox unit consists mainly of a several-km thick sequence of medium grade, graphite-bearing schists and metapsammites, which are locally underlain by small bodies of muscovite-bearing leucogneisses. The schists have a monotonous appearance and show no major breaks in bulk composition (Table 1; cf. García-Casco and Torres Roldán, 1996), except near the contact with the gneisses, where they become richer in plagioclase and locally contain cm- to mm-sized segregations of trondhjemitic composition (Pl + Qtz, lacking K-feldspar). Structural development consists of a main foliation (S_2) that transposes early structures and is associated with small-scale subhorizontal tight folds. The S_2 foliation is deformed by D_3 folds, and a differentiated crenulation foliation S_3 transposes S_2 locally (Cuevas et al. 1989).

Mineral assemblages going upgrade in the metapelites of the Torrox unit include: (1) St + Bt + Grt + And (Andalusite schists); (2) St + Bt + Grt + Fib + And (Fibrolite schists); (3) St + Bt + Grt + Ky + Fib + And (Kyanite schists). Cordierite occasionally joins any of these assemblages (Fig. 1). The growth of the key AFM phases relative to the main stages of deformation was pre-D_2 for kyanite and garnet, pre-D_2 and syn-D_2 for staurolite, syn-D_2 for fibrolite, post-D_2 to syn-D_3 for andalusite and post-D_3 for cordierite (García-Casco and Torres-Roldán 1996). To be noted is that some of the higher grade metapelites display post-D_3 recrystallization that obscure D_2 and D_3 microstructures. In these samples, kyanite, fibrolite, garnet and staurolite, otherwise abundant in this type of rock, are scarce or absent. All assemblages contain quartz, muscovite, plagioclase, rutile and ilmenite, with tourmaline, apatite and (less commonly) Fe-sulphides occurring locally. Chlorite is also found in some rocks as retrograde grains that replace biotite, garnet and staurolite. The more prominent textural and compositional features in the Torrox metapelites developed during D_{2-3}, and include: (1) sequential growth of Ky → Fib → And; (2) replacements of garnet by combinations of St, Bt, Fib, And, Pl and Ilm; (3) replacements of staurolite by combinations of Bt, Fib, And and Ilm; (4) the replacement of rutile by ilmenite; (5) wide compositional heterogeneity in the micas and plagioclase related to textural placement; (6) anomalous Mg-Fe partitioning between biotite-garnet and staurolite-garnet pairs (indicated by odd thermometric results and reverse Fe-Mg partitioning, i.e. $X_{Fe}^{St} > X_{Fe}^{Grt}$, respectively). García-Casco and Torres-Roldán (1996) related these features to the overstepping of equilibrium boundaries during post-peak near-isothermal decompression (from >10 kbar down to 2–3 kbar, at an estimated rate of 5–10 km/Ma). Previous to decompression, the *P-T* path of the Torrox schists was characterized by clockwise heating (up to 650 °C at ≈8–10 kbar), followed by compression up to 12 kbar at peak *T*.

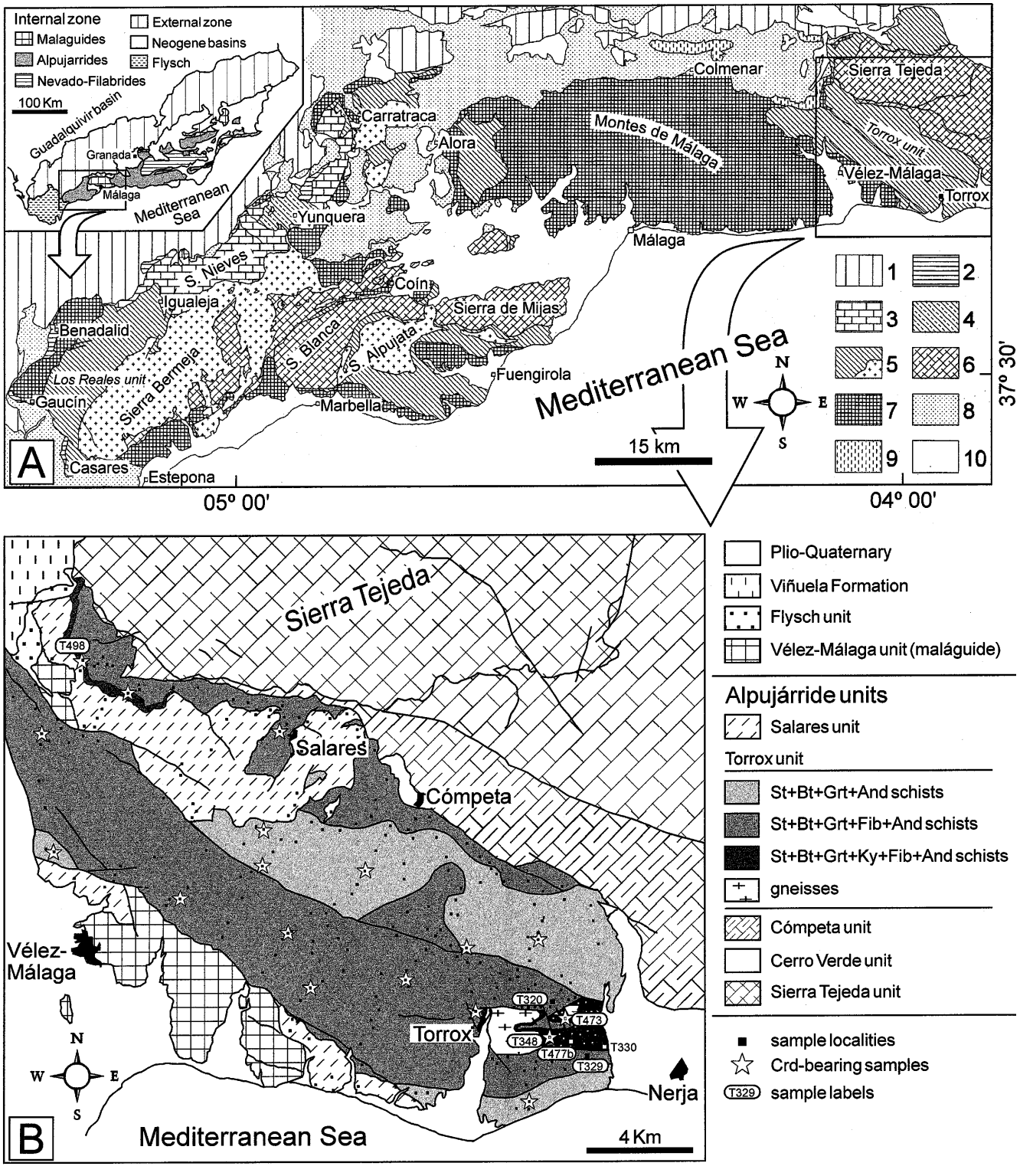

Cordierite-bearing rocks

The appearance of cordierite in the Torrox schists is not related to metamorphic grade, as indicated by the fact that cordierite-bearing samples have a random field distribution (Fig. 1) and are associated to cordierite-lacking samples at the scale of single outcrops. When present, cordierite is rather seen to join the And + Bt pair that overprints higher pressure assemblages in all types of schists, and a plot of bulk compositions (Fig. 2) suggests that the main control on cordierite growth was related to subtle variations of FeO/(FeO + MgO) bulk ratios. Cordierite appears mostly in the form of cryptocrystalline aggregates (pinite) where crystalline areas of cordierite are rarely preserved. In all samples cordierite is seen to replace pre-existing garnet and staurolite porphyroblasts, but cordierite relations are generally obscured by the concurrence of other

Table 1 XRF analyses of metapelite samples from the Torrox unit

Sample	T320	T329	T330	T477B	T348	T473
Zone	Fibrolite schists		Kyanite schists			
	Crd-lacking		Crd-lacking		Crd-bearing	
Oxide proportions (wt%)						
SiO_2	65.00	67.08	68.16	59.40	66.10	73.50
TiO_2	0.90	0.83	0.77	0.96	0.81	0.75
Al_2O_3	17.44	17.03	16.80	20.70	16.00	12.40
FeO	5.68	5.34	4.92	6.90	5.23	4.29
MnO	0.09	0.08	0.07	0.11	0.09	0.07
MgO	1.64	1.58	1.35	1.81	1.78	1.53
CaO	0.94	0.77	1.00	0.54	1.69	1.36
Na_2O	1.38	1.39	1.72	0.55	1.87	1.42
K_2O	3.00	3.07	2.47	3.95	2.76	2.03
P_2O_5	0.19	0.13	0.15	0.24	0.16	0.13
Loss on ignition	3.14	2.46	2.63	4.08	2.62	2.08
Total	99.39	99.76	100.05	99.24	99.11	99.56
FeO/(FeO + MgO)	0.776	0.772	0.785	0.792	0.746	0.737

replacements of garnet and staurolite consisting of combinations of Fib-And-Bt-Ms-Ilm-Pl that developed during decompression, previous to cordierite growth (García-Casco and Torres-Roldán 1996). In a few rocks, however, the latter types of replacements are scarce, and one of such sample was hence chosen for detailed study. This sample, T348, is a massive schist with enhanced post-D_3 recrystallization, and displays a variety of reaction textures involving cordierite growth after garnet, staurolite and, interestingly too, after muscovite and earlier biotite. Further, the rock contains some fresh cordierite areas within pinite, and lacks kyanite and fibrolite. The EPMA data (Table 2, BSE and X-ray images) were collected with a CAMEBAX SX50 machine at the University of Granada. The reader is referred to García-Casco et al. (1993) for details on the analytical procedures.

Reaction textures (cordierite-bearing replacement textures)

Garnet porphyroblasts (0.5–1 mm in diameter, with inclusions of quartz and rutile) are corroded by fine grained aggregates of Crd + Bt + Ilm + Qtz + Pl that form 0.1–0.4 mm thick coronas (Fig. 3A). The replacements also progress along fractures within garnet (Figs. 3A and 4), suggesting the presence of a fluid phase during replacement. Less commonly, garnet is also replaced by simpler mixtures of Bt + Ms. *Staurolite* is replaced by aggregates of Crd + Bt + Ilm (Fig. 3E). Within these replacements, staurolite appears as fine xenomorphic grains that are often arranged in optical continuity, indicating that they are relicts of larger porphyroblasts. Locally, adjacent grains of garnet and staurolite develop continuous replacements which indicate that both phases were involved in the cordierite-forming event. Early *muscovite* plates of 1–2 mm in size appear deformed and corroded by Crd + Bt + Qtz ± Ilm ± Pl (Figs. 3E, G and H), where the grains of biotite, cordierite and quartz are often intergrown parallel to the (0 0 l) planes of the host muscovite (Figs. 3G and H). Cordierite-bearing intergrowths are nonetheless absent in finer and texturally younger muscovite laths that are dispersed in the matrix or replacing garnet (in the Bt + Ms replacements) and plagioclase porphyroblasts. *Rutile* is located within garnet porphyroblasts and dispersed in the matrix, and matrix grains are replaced by ilmenite.

In addition to the small grains that replace garnet, staurolite and muscovite, *biotite* plates 1–2 mm in size, which contain patches of fine grained Crd + Ilm + Qtz (Fig. 3C and D), are dispersed in the matrix. These patches are comparable and often overlap with those developed after garnet (Fig. 3A and B), but textural criteria are ambiguous as to whether this type of biotite is replaced by Crd + Ilm + Qtz aggregates or both are products of Crd-forming reactions. The development of diffusion zoning in biotite plates next to the patches, however, indicates that these biotites were reacting to Crd + Ilm + Qtz while Bt + Crd was being produced in adjacent reaction sites after garnet, staurolite and muscovite.

Andalusite appears in sample T348 as dispersed porphyroblasts with inclusions of biotite and ilmenite and as aggregates intergrown with biotite. Andalusite is systematically absent in cordierite-bearing replacements, however, and wherever it is in contact with cordierite the phase boundary is clean (Fig. 3F). The same relationships are present in other cordierite-bearing samples from the Torrox unit, even if fibrolite and kyanite are also coexisting phases. In general, the textures indicate that andalusite was not involved in the reaction processes that led to cordierite growth, either as re-

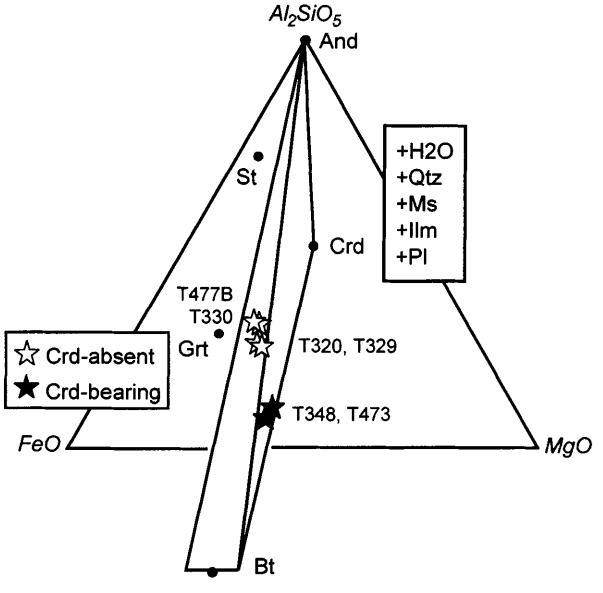

Fig. 2 AFM projection of whole rock compositions (Table 1) and representative compositions of the phases coexisting in sample T348. The *fields* for the assemblages And + Bt and And + Bt + Crd developed at low *P* in the cordierite-absent and cordierite-bearing samples, respectively, have been drafted for reference. Note that cordierite-bearing schists have slightly lower FeO (FeO + MgO) ratios

Table 2 Representative compositions of minerals from sample T348

	Staurolite relicts		Garnet				Ilmenite			
			Core[d]		Rims		Matrix	Product after		
			(a)	(b)	High-Ca	retrogr.[e]		Grt(1)[f]	St(1)[f]	Ms(1)[f]
SiO_2	27.07	26.87	37.01	37.91	38.15	37.03	–	–	–	–
TiO_2	0.71	0.70	0.02	0.01	0.10	0.01	53.00	52.71	52.81	53.01
Al_2O_3	54.48	55.29	20.71	21.32	21.33	21.05	0.00	0.00	0.00	0.00
Cr_2O_3	–	–	0.03	0.00	0.01	0.00	0.01	0.01	0.00	0.01
FeO[a]	12.97	12.92	32.58	32.59	28.61	33.81	43.42	44.89	44.18	44.27
MnO	0.25	0.27	5.31	1.56	0.34	3.52	2.99	1.66	2.25	2.40
ZnO	0.75	0.73	–	0.01	–	0.00	0.02	0.00	0.00	0.06
MgO	1.22	1.20	2.19	5.18	5.35	2.81	0.02	0.00	0.00	0.01
CaO	–	–	2.01	1.72	6.29	1.74	–	–	–	–
Total	97.45	97.98	99.86	100.31	100.18	99.97	99.44	99.27	99.24	99.76
	Si + Al = 25.53[b]		12 O pfu				6 O pfu			
Si	7.571	7.453	3.004	2.999	2.991	2.990	–	–	–	–
$^{[IV]}Al$	0.429	0.547	0.000	0.001	0.009	0.010	–	–	–	–
$^{[VI]}Al$	17.530	17.530	1.981	1.987	1.961	1.993	0.000	0.000	0.000	0.000
Cr	–	–	0.002	0.000	0.001	0.000	0.000	0.001	0.000	0.000
Ti	0.148	0.147	0.001	0.001	0.006	0.001	2.017	2.012	2.015	2.013
Fe^{2+}	3.033	2.997	2.211	2.156	1.875	2.283	1.837	1.905	1.874	1.869
Mn	0.059	0.063	0.365	0.105	0.023	0.241	0.128	0.071	0.097	0.103
Zn	0.155	0.150	–	0.001	–	0.000	0.001	0.000	0.000	0.002
Mg	0.509	0.495	0.264	0.611	0.625	0.338	0.001	0.000	0.000	0.000
Ca	–	–	0.175	0.145	0.528	0.151	–	–	–	–
H^{+c}	3.734	3.960								
Fe/Fe + Mg	0.856	0.858	0.893	0.779	0.750	0.871	0.999	1.000	1.000	1.000
Mn/Mn + Fe	0.019	0.021	0.142	0.046	0.012	0.095	0.065	0.036	0.049	0.052
X_{alm}			0.733	0.715	0.615	0.758				
X_{sps}			0.121	0.035	0.007	0.080				
X_{prp}			0.088	0.203	0.205	0.112				
X_{grs}			0.058	0.048	0.173	0.050				

	Biotite						Muscovite			
	Matrix		Product after				Porphyroblast		Product after	
	Core	Retrogr	Grt(1)[h]	Grt(2)[h]	St(1)[h]	Ms(1)[h]	High-Si	Low-Si	Grt(2)[h]	Pl
SiO_2	35.44	35.12	35.61	34.55	35.31	35.06	49.40	46.07	46.52	47.14
TiO_2	2.65	3.56	4.02	0.36	4.57	3.45	1.18	0.50	0.36	0.02
Al_2O_3	20.03	19.76	19.58	21.75	19.07	19.49	30.54	36.43	36.22	36.19
Cr_2O_3	0.05	0.06	0.06	0.03	0.04	0.07	0.08	0.00	0.03	0.04
FeO	21.17	21.41	22.33	21.55	21.02	22.30	2.01	0.85	1.00	0.81
MnO	0.17	0.21	0.15	0.17	0.12	0.19	0.03	0.01	0.00	0.00
ZnO	–	0.02	–	–	–	–	–	–	–	–
MgO	7.07	6.83	6.05	7.64	6.42	6.39	1.90	0.38	0.55	0.59
CaO	0.01	0.00	0.01	0.00	0.01	0.02	0.00	0.02	0.00	0.01
Na_2O	0.25	0.15	0.22	0.20	0.20	0.22	0.32	0.54	0.53	0.50
K_2O	8.21	8.50	8.16	7.94	8.32	8.24	9.56	9.98	10.13	10.06
Total	95.05	95.63	96.19	94.19	95.08	95.43	95.02	94.78	95.34	95.36
	20 O, 4 OH pfu						20 O, 4 OH pfu			
Si	5.406	5.348	5.395	5.317	5.394	5.369	6.562	6.125	6.155	6.217
$^{[IV]}Al$	2.594	2.652	2.605	2.683	2.606	2.631	1.438	1.875	1.845	1.783
$^{[VI]}Al$	1.007	0.895	0.892	1.263	0.828	0.886	3.345	3.832	3.804	3.842
Cr	0.007	0.008	0.007	0.003	0.005	0.008	0.008	0.000	0.003	0.004
Ti	0.304	0.408	0.458	0.042	0.524	0.398	0.118	0.050	0.035	0.002
Fe^{2+}	2.701	2.727	2.829	2.774	2.685	2.855	0.223	0.094	0.110	0.089
Mn	0.022	0.026	0.019	0.023	0.016	0.024	0.003	0.001	0.000	0.000
Zn	–	0.002	–	–	–	–	–	–	–	–
Mg	1.608	1.551	1.368	1.753	1.463	1.459	0.376	0.075	0.108	0.117
Σ[VI][g]	5.649	5.618	5.573	5.858	5.521	5.630	4.073	4.052	4.060	4.054
Ca	0.001	0.000	0.002	0.000	0.001	0.003	0.000	0.003	0.000	0.002
Na	0.074	0.043	0.066	0.059	0.059	0.064	0.082	0.140	0.136	0.127
K	1.597	1.652	1.577	1.559	1.622	1.610	1.620	1.692	1.709	1.692
Σ[XII][g]	1.672	1.696	1.645	1.618	1.682	1.677	1.702	1.835	1.845	1.821
Fe/Fe + Mg	0.627	0.637	0.674	0.613	0.647	0.662	0.372	0.556	0.505	0.432
Mn/Mn + Fe	0.008	0.009	0.007	0.008	0.006	0.008	0.013	0.011	0.000	0.000

Table 2 (continued)

	Cordierite product after				Plagioclase		
	St (fresh)	Bt (fresh)	Grt[i]	Ms[i]	Porph. core	Matrix	After Grt
SiO_2	48.23	47.73	41.13	39.70	63.91	60.88	59.47
TiO_2	0.01	0.02	0.57	0.00	–	–	–
Al_2O_3	32.63	34.80	26.67	35.73	22.86	24.94	25.85
Cr_2O_3	0.01	0.04	0.03	0.00	–	–	–
FeO	10.14	9.22	12.00	7.66	–	–	–
MnO	0.34	0.45	0.21	0.20	–	–	–
ZnO	0.01	0.03	0.02	0.01	–	–	–
MgO	6.77	5.74	4.29	3.70	–	–	–
CaO	0.06	0.30	1.23	0.89	4.25	6.71	7.99
Na_2O	0.41	0.34	0.83	0.38	8.75	7.64	6.95
K_2O	0.02	0.27	4.04	0.58	0.49	0.33	0.27
Total	98.61	98.94	91.02	88.84	100.25	100.50	100.53
	18 O pfu				8 O pfu		
Si	5.004	4.922	4.883	4.571	2.816	2.696	2.641
Al	3.990	4.229	3.731	4.848	1.187	1.302	1.353
Cr	0.001	0.003	0.003	0.000	–	–	–
Ti	0.001	0.001	0.051	0.000	–	–	–
Fe^{2+}	0.880	0.795	1.191	0.737	–	–	–
Mn	0.030	0.039	0.021	0.019	–	–	–
Zn	0.000	0.002	0.002	0.000	–	–	–
Mg	1.046	0.883	0.759	0.635	–	–	–
Ca	0.006	0.034	0.157	0.109	0.200	0.318	0.380
Na	0.082	0.068	0.190	0.085	0.747	0.656	0.598
K	0.002	0.035	0.612	0.085	0.027	0.019	0.015
Fe/Fe + Mg	0.457	0.474	0.611	0.537	–	–	–
Mn/Mn + Fe	0.033	0.047	0.017	0.025	–	–	–

[a] Total Fe as FeO. (unaccounted Fe^{3+} must be low in presence of graphite, which imposes low fo_2 conditions and hence low Fe^{3+}/Fe^{2+} ratios in the micas; e.g. Guidotti and Dyar, 1991)
[b] Staurolite formula calculated on the basis of Si + Al = 25.53 atoms pfu and total positive charge = 96 after the suggestion of Holdaway et al. (1986) for graphite-bearing rocks
[c] H^+ content in staurolite calculated by stoichiometry
[d] (*a*) Denotes core, (*b*) the interior of grains adjacent to high-Ca overgrowths
[e] *Retrogr*: the interiors exposed due to replacement of high-Ca rims and modified by diffusion
[f] (*1*) Refers to Crd + Bt + Ilm replacements
[g] Σ[VI] and Σ[XII] refer to octahedral and interlayer occupancies, respectively
[h] (*1*) Biotite of Crd + Bt + Ilm replacements after garnet, staurolite and high-Si muscovite, (*2*) biotite and low-Si muscovite from Bt + Ms replacements after garnet
[i] Pinite analyses

actant or product, and suggest that andalusite was formed previous to cordierite growth.

Mineral compositions

Garnet porphyroblasts display normal (i.e. growth) zoning, with Fe/(Fe + Mg) ($=X_{Fe}$) and Mn decreasing from core to rim, except for 10–20 μm wide diffusional rims that develop along the contacts with the replacements. Within the diffusional rim both X_{Fe} and Mn increase (Fig. 4), indicating that temperature and/or pressure decreased during garnet replacement. The Ca content is low and homogeneous ($X_{grs} \approx 0.05$), except in some protuberances or isolated garnet remnants within the coronas where it increases noticeably (up to $X_{grs} = 0.174$, Fig. 4). These high-Ca rims have low Mn and X_{Fe} and can be correlated with better preserved high-Ca overgrowths in garnets from cordierite-absent metapelites, where they record the peak pressure conditions attained in the Torrox unit (10–12 kbar, García-Casco and Torres-Roldán 1996). The near complete obliteration of these Ca-rich rims in sample T348 indicates that advanced dissolution of garnet took place during cordierite growth. *Staurolite* composition is fairly homogeneous [$X_{Fe} = 0.845–0.858$, Mn/(Fe + Mn) = 0.019–0.023] in sample T348, with no clear indication of zoning (Fig. 5). However, better preserved staurolite porphyroblasts from other cordierite-bearing samples display a slight increase in X_{Fe} and Mn towards the rims, next to the replacements (Fig. 5), suggesting that some diffusional exchange accompanied staurolite replacement. *Muscovite* displays a wide compositional heterogeneity, which corresponds with textural type. The early (reacting) crystals of muscovite have higher Si,

▶

Fig. 3A–H Representative textures of cordierite growth in sample T348: **A** Optical image of pinite + biotite replacement after garnet and adjacent plate of biotite (the *inset* shows the same image at a lower scale). **B** BSE image of the *box* in **A** showing the presence of relict biotite (*white*) within heterogeneous pinite material (*gray-shaded*). **C** Matrix biotite plate replaced by fine grained Crd + Qtz + Ilm aggretates. **D** BSE image of the area shown in **C** that illustrates the nature of the replacements, with fresh cordierite within pinite material. The *line* marks the location of the composition profile along the biotite plate that is shown in Fig. 8. **E** Optical image of staurolite relicts within cordierite + biotite + ilmenite aggregates. A muscovite plate with replacements is within view, as well as clearer neoformed low-Si muscovite crystals that appear (*lower-left corner*) in the replacement aggregate. **F** Optical image of andalusite porphyroblast in contact with pinite aggregate. Both, the sharp contact among andalusite and pinite and that pinite adapts to andalusite rims, suggest that cordierite growth followed that of andalusite. **G** BSE image of muscovite plate replaced by cordierite (pinite), biotite and quartz running parallel to the (0 0 l) planes of muscovite. Note the heterogeneous composition of muscovite (*black arrows* point to low-Si muscovite areas, that appear *darker* in the image). **H** Detailed BSE image of the area shown in **G** illustrating the distribution of Fe across the intergrown assemblage (*white line*). Note the heterogeneous nature of pinite

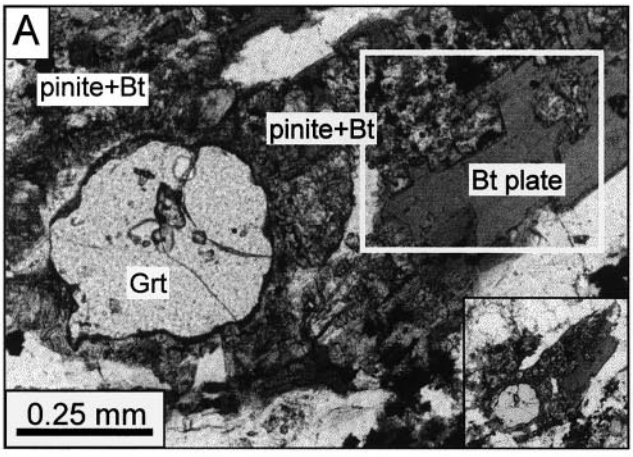
A
pinite+Bt
pinite+Bt
Bt plate
Grt
0.25 mm

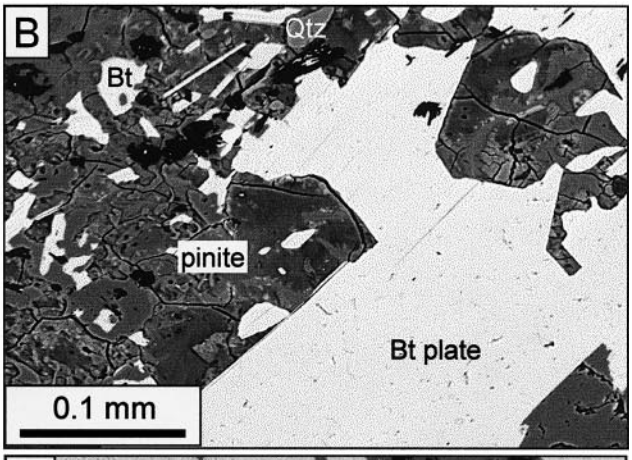
B
Qtz
Bt
pinite
Bt plate
0.1 mm

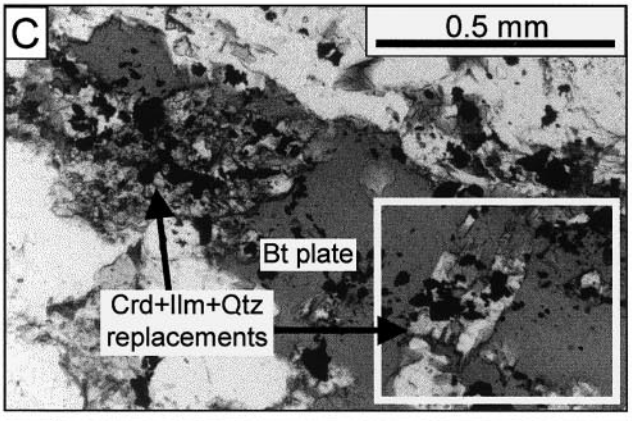
C
0.5 mm
Bt plate
Crd+Ilm+Qtz
replacements

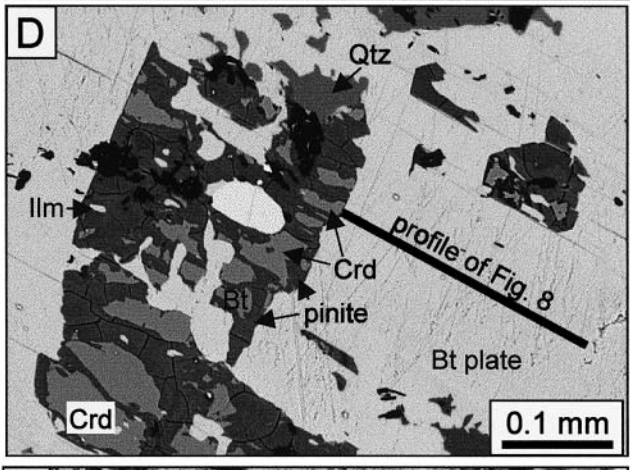
D
Qtz
Ilm
profile of Fig. 8
Crd
Bt
pinite
Bt plate
Crd
0.1 mm

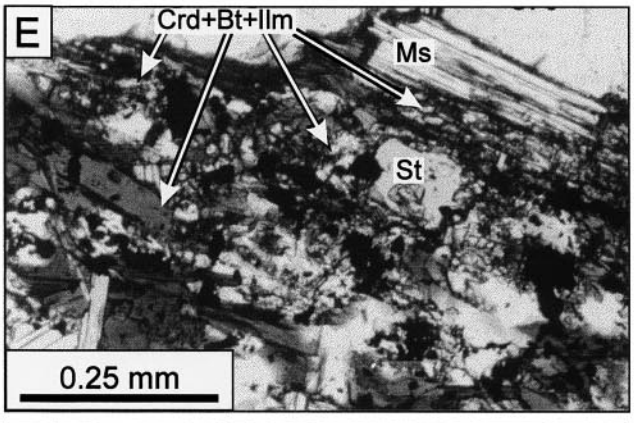
E
Crd+Bt+Ilm
Ms
St
0.25 mm

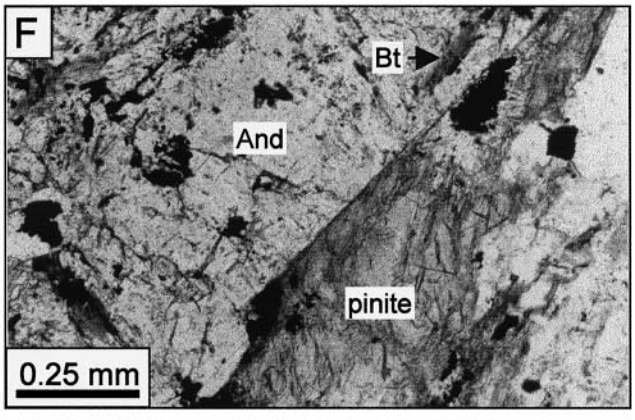
F
Bt
And
pinite
0.25 mm

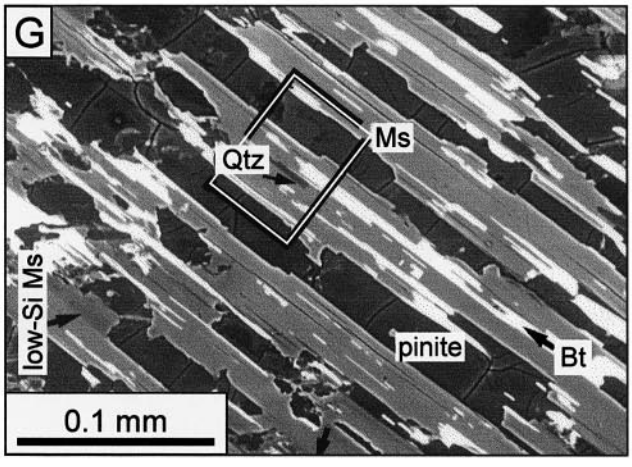
G
Qtz
Ms
low-Si Ms
pinite
Bt
0.1 mm

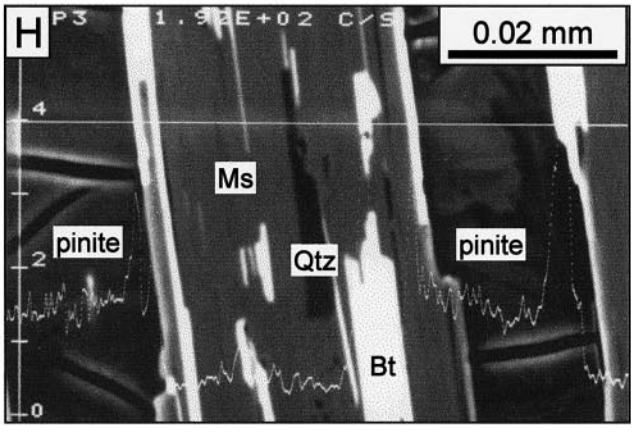
H
0.02 mm
Ms
pinite
Qtz
pinite
Bt

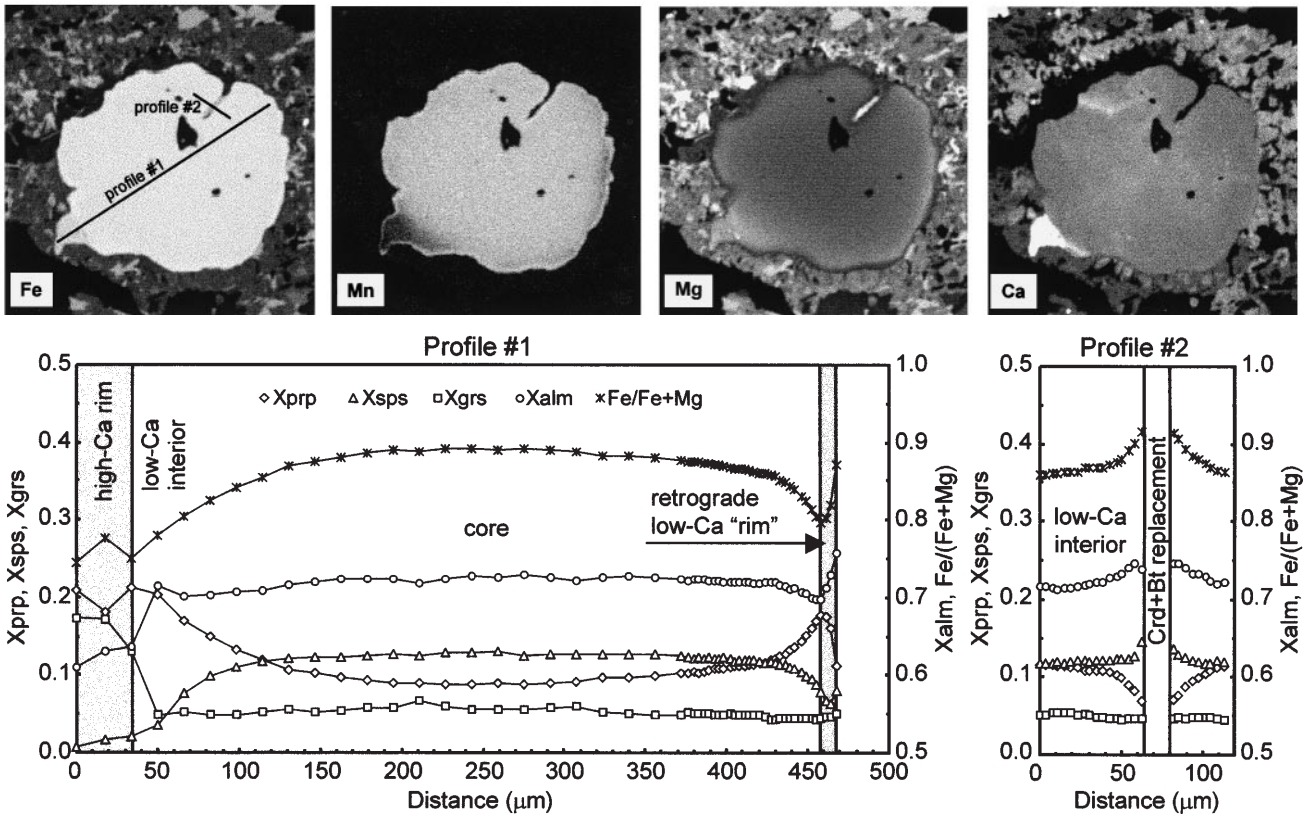

Fig. 4 Zoning of the replaced garnet porphyroblast shown in Fig. 3A, illustrated by X-ray maps of the distribution of Fe, Mn, Mg, and Ca, and X_{alm}, X_{sps}, X_{prp}, X_{grs}, and Fe/(Fe + Mg) traverses along (1) the replaced high-Ca rim to replaced low-Ca "rim" and (2) the replaced low-Ca interior. In the X-ray images, *white and black* correspond to high and low elemental concentration, respectively. The composition of garnet is modified by diffusion [upturns in Fe, Mn, Mg and Fe/(Fe + Mg)] adjacent to the replacements, except in the relict fragments of the high-Ca rim of the porphyroblasts

Fe, Mg, Ti, octahedral occupancy, and interlayer vacancy, and lower $^{[IV]}$Al, $^{[VI]}$Al, K, Na, and X_{Fe} than the younger muscovites dispersed in the matrix or replacing garnet and plagioclase (Fig. 6). This trend, which essentially involves the Tschermak substitution, is also observed within single crystals of high-Si muscovite, which was interpreted as the result of muscovite re-equilibration during decompression by García-Casco et al. (1993).

Biotite also shows large compositional variations associated to textural placement (Fig. 7), particularly in the octahedrally coordinated cations ($^{[VI]}$Al = 0.789–1.293, Ti = 0.040–0.524, Fe = 2.597–2.966, Mg = 1.356–1.753 and Σ[VI] = 5.507–5.858). The grains from Bt + Ms replacements after garnet have high $^{[VI]}$Al and low Ti and X_{Fe}, and are likely largely deviated from equilibrium given that the production of ilmenite at the time of cordierite growth requires biotite to be saturated in Ti (cf. Guidotti et al. 1977). Further, these grains are notable in that they have $^{[VI]}$Al > 1 atoms per formula unit (p.f.u.), which exceeds the expectations for metamorphic biotites (cf. Guidotti 1984). Matrix biotite plates are intermediate in composition, with X_{Fe} in the range 0.612–0.643, and the lowest $^{[VI]}$Al, and highest Ti and X_{Fe} (0.667–0.677 and 0.647–0.650 for replacements after garnet and staurolite, respectively) are from the grains in the Crd + Bt + Ilm replace-

Fig. 5 Bivariate diagrams showing the chemical heterogeneity of relict staurolite grains from sample T348 and sample T498, a Crd + Ky-bearing metapelite where larger staurolite porphyroblasts are replaced by Crd + Bt

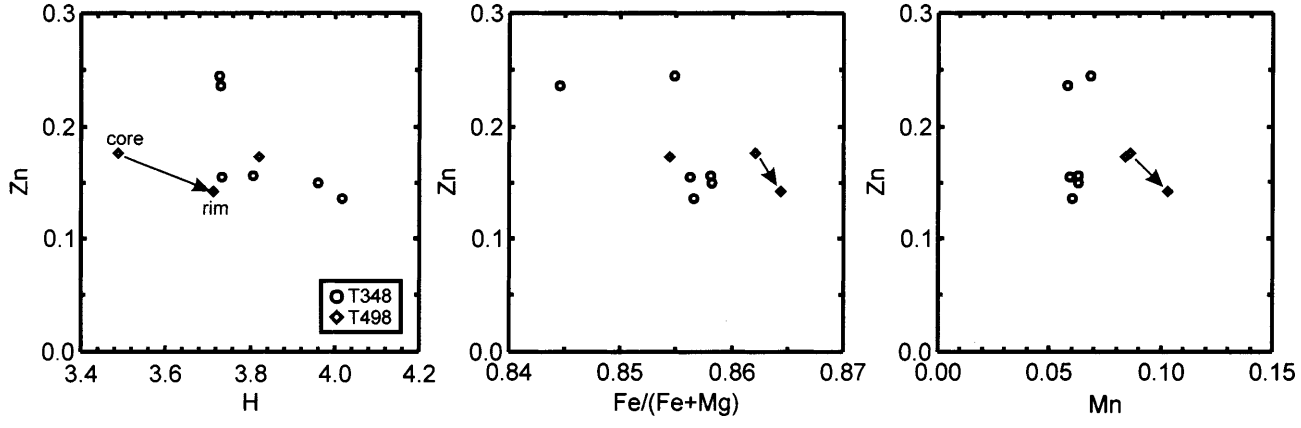

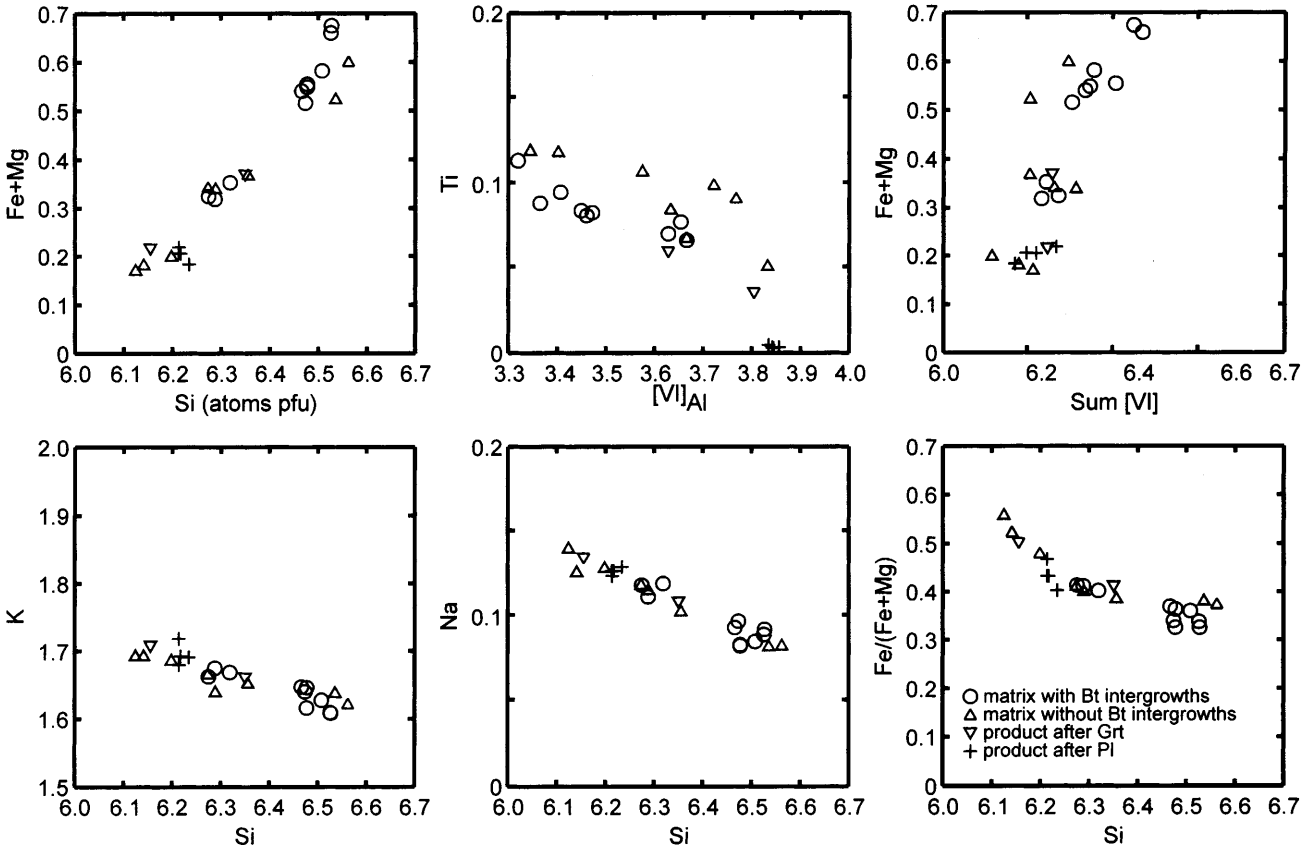

Fig. 6 Bivariate diagrams showing the large chemical heterogeneity of muscovite. Note the high Si, Fe and Mg contents of relict muscovite replaced by Crd + Bt + Qtz, and that the composition trend is largely controlled by the Tschermak substitution

ments. These variations are indicators of severe diffusion problems between different reaction sites, the more so when it seems likely that a fluid phase had been present at the time of cordierite growth. The severity of diffusion problems is further illustrated by the occurrence of zoned rims in plates of matrix biotite, which involve increasing Ti, Fe and X_{Fe}, and decreasing Mg and $^{[VI]}Al$, towards the patches of Crd + Ilm + Qtz (Fig. 8). Though subtle, this zoning is significant in that it matches the trend of biotites from the Crd + Bt + Ilm replacements after garnet, staurolite, and muscovite (Fig. 7), suggesting that matrix biotite (with lower Ti and X_{Fe}) changed its composition (towards higher Ti and X_{Fe}) as it was replaced by the Crd + Ilm + Qtz aggregates. This process is similar to that of garnet replacement, although remarkable given

Fig. 7 Bivariate diagrams illustrating the chemical heterogeneity of biotite. Note the increase in Ti and Fe/(Fe + Mg) and the decrease in $^{[VI]}Al$ in the grains from Crd + Bt + Ilm replacements after garnet and staurolite, as opposed to the grains from the Bt + Ms replacements after garnet

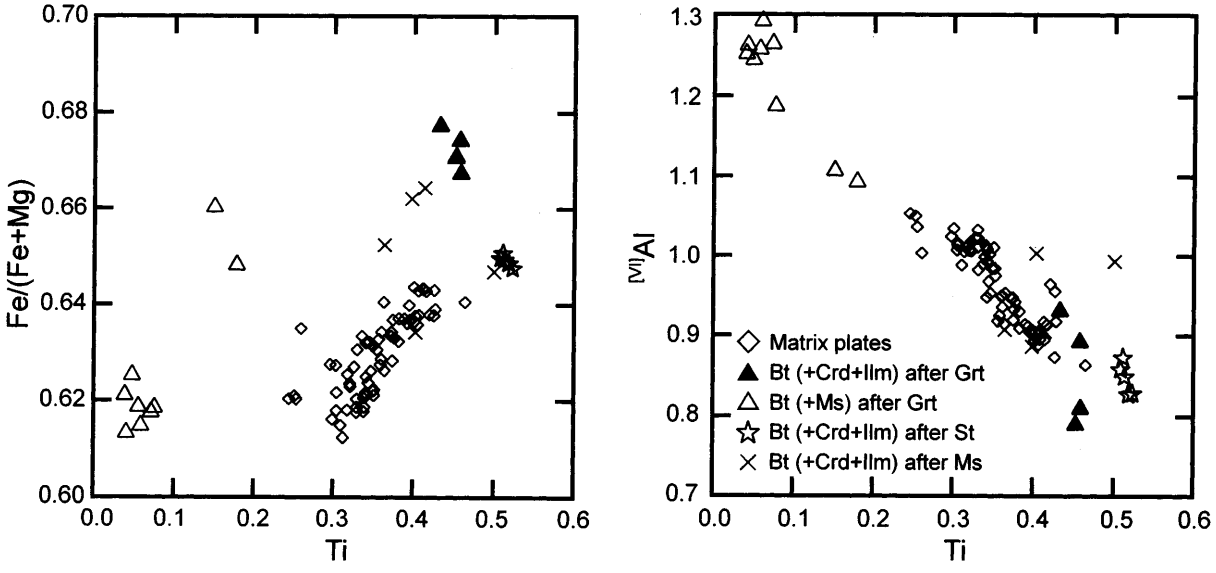

the much faster nature of cation diffusion in biotite relative to garnet (e.g. Dowty 1980; Spear 1991; Florence and Spear 1991; Pattison 1994; Gessmann et al. 1997). The preservation of delicate zoning in these biotites is consistent with the onset of fast cooling immediately after cordierite growth, in agreement with the thermochronological constraints reviewed in the introductory section.

Fresh *cordierite* was found only as fine inclusions within the pinite material from some replacements after staurolite and the matrix plates of biotite. In the staurolite replacements cordierite has X_{Fe} = 0.450–0.465 and Mn/(Fe + Mn) = 0.028–0.035, slightly lower than in the grains associated to matrix biotite (0.474–0.477 and 0.047, respectively; Fig. 11). The oxide sums in all cases are ca. 98.5 wt%, indicating some hydrous ($\pm CO_2 \pm CH_4$) component. *Ilmenite* is also heterogeneous, with variable Mn/(Fe + Mn) that is higher in matrix grains (0.062–0.065) and lower in the replacements, down to 0.036–0.045 in the replacements after garnet (Fig. 9). A relevant feature of all types of ilmenite grains is that no Fe^{3+} can be calculated on the basis of stoichiometric constraints, which might be taken as an indication of low f_{O_2} conditions during metamorphism. Finally, *plagioclase* from the replacements after garnet has distinctly lower Na contents (X_{ab} = 0.602–0.608) than porphyroblasts (0.709–0.761; Fig. 10).

Evidences of disequilibrium

Besides compositional heterogeneity of all the phases, other evidences of chemical disequilibrium in sample T348 relate to Fe-Mn-Mg partitioning among the coexisting phases (Fig. 11), and these are relevant in that they help constraining the reaction history of the rock during, and previous to, cordierite growth. The sequence of X_{Fe} [= Fe/(Fe + Mg)] and X_{Mn} [= Mn/(Mn + Fe)] in the coexisting phases is $X_{Fe}^{Ilm} > X_{Fe}^{Grt(retrograde\ ``rims'')} > X_{Fe}^{Grt(core)} > X_{Fe}^{St} > X_{Fe}^{Grt(low\text{-}Ca\ interiors)} > X_{Fe}^{Grt(high\text{-}Ca\ rim)} > X_{Fe}^{Bt} > X_{Ms}^{Ms(low\text{-}Si)} > X_{Fe}^{Crd} > X_{Ms}^{Ms(high\text{-}Si)}$, and $X_{Mn}^{Grt(core)} > X_{Mn}^{Grt(retrograde.``rims'')} > X_{Mn}^{Ilm} \geq X_{Mn}^{Grt(low\text{-}Ca\ interiors)} > X_{Mn}^{Crd} > X_{Mn}^{St} > X_{Mn}^{Grt(high\text{-}Ca\ rim)} > X_{Mn}^{Bt} \approx X_{Mn}^{Ms}$. These relationships show a number of conflicts with theory, experiments, and observations in natural Fe-rich metapelites worldwide. Among these, the inverse Fe-Mg partitioning between garnet and staurolite ($X_{Fe}^{St} > X_{Fe}^{Grt(low\text{-}Ca\ interiors)} > X_{Fe}^{Grt(high\text{-}Ca\ rim)}$) stands out since the composition of the rock is Fe-rich, and equilibrium $X_{Fe}^{St} > X_{Fe}^{Grt}$ occurs only in Mg-rich systems (Ganguly and Saxena 1987; see also García-Casco and Torres-Roldán 1996 p. 1220). These high-Ca garnet rims also have X_{Mn} lower than staurolite, ilmenite, and cordierite, that conflicts with expectations (Thompson 1976a; Feenstra and Engi 1998; Spear and Cheney 1989; Powncby et al. 1987, 1991; Symmes and Ferry 1992). Staurolite and cordierite display normal Fe-Mg and Fe-Mn partitioning, but inverse Mn partitioning is apparent in the Fe-Mg-Mn system [i.e. $Mn/(Fe + Mg + Mn)^{Crd} < Mn/(Fe + Mg + Mn)^{St}$].

Normal Fe-Mg partitioning is apparent between the high-Ca garnet rims and all types of biotite (Fig. 11), but the results of thermometry using the associated partition coefficients are conflicting in that they are unreasonably high (900–1200 °C for matrix biotite, Fig. 12A, and still higher for biotite from Crd + Bt replacements). The GASP barometer yields ca. 12 kbar (at 600–650 °C) for these relict high-Ca garnet rims (using Na-rich plagioclase and kyanite; Fig. 12A), suggesting that the high-Ca garnet rims grew at high *P*. The temperatures calculated

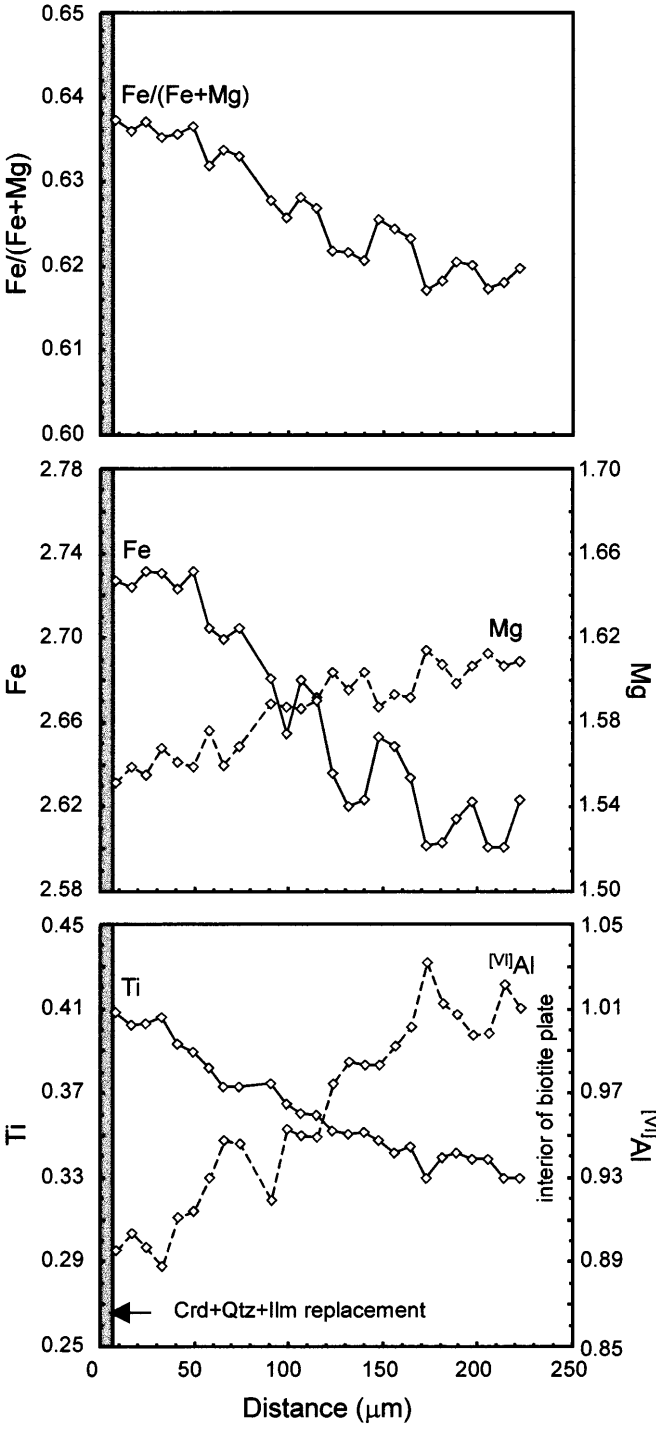

Fig. 8 Element distribution in the biotite plate with Crd + Ilm + Qtz replacements shown in Fig. 3D. Note the increase in Ti and Fe/(Fe + Mg) and the decrease in $^{[VI]}Al$ and Mg towards the replacement, similar to the trend of biotites from Crd + Bt + Ilm replacements after garnet and staurolite shown in Fig. 7

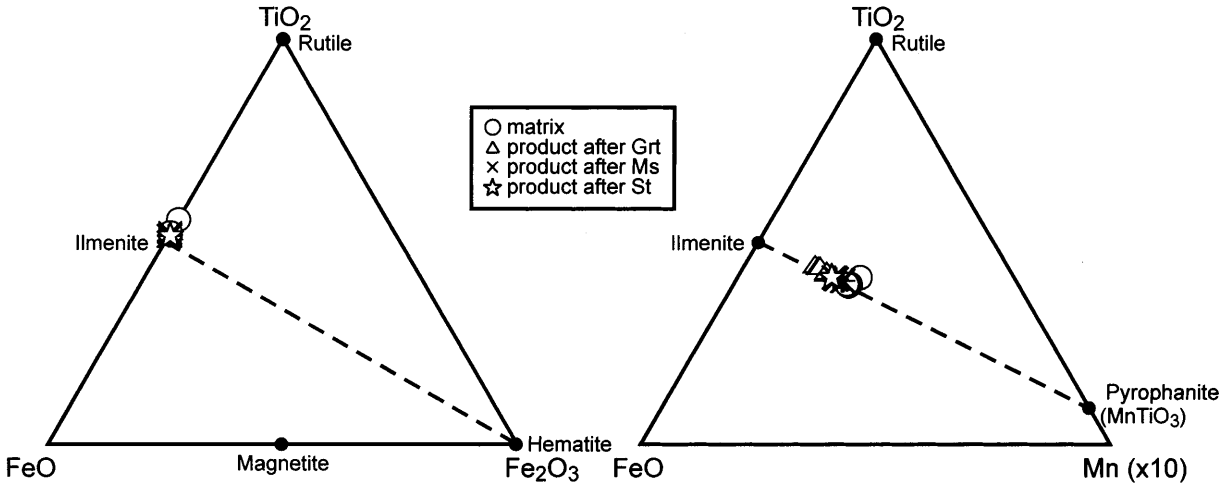

Fig. 9 Ternary diagrams showing the compositional heterogeneity of ilmenite. Note the low hematite content of the analysed grains

with the Grt-Bt and Grt-Crd Fe-Mg exchange thermometers using the diffusional rim of garnet, whose composition was attained at low P during cordierite growth, in addition to high-Ti biotite and cordierite from the replacements are still very high (> 700 °C; Fig. 12B and C), pointing out that even the composition of retrograde garnet is not wholly equilibrated with product biotite and cordierite. The Crd-Bt Fe-Mg exchange, although notoriously poor as a reliable thermometer (e.g. Pattison and Tracy 1991), yields satisfactory though imprecise results (in the range 450–600 °C; Fig. 12D).

From the equilibrium point of view, the picture that emerges from these relationships is chaotic, because generalized disequilibrium is not only detected between reactants and products, but also among the reactants (i.e. garnet, staurolite and matrix biotite). That the reactants did not coexist at equilibrium suggests that cordierite growth was preceded during decompression by a reaction history during which large overstepping of several equilibrium surfaces had taken place. This history, that culminated at low P with the reactions that produced cordierite, is discussed next.

Reaction history

P-T path and P-T-X_{H_2O} conditions of cordierite growth

Figure 12 shows a variety of P-T results for sample T348 obtained using the TWQ software (v. 2.02) of Berman (1991). The P-T path proposed by García-Casco and Torres-Roldán (1996) for the kyanite-bearing metapelites of the Torrox unit is drawn for reference. This path consists of four stages: (1) heating (ΔT > 150 °C) with moderate pressure decrease ($\Delta P \approx -2$ kbar) within the kyanite stability field; (2) compression up to ca. 12 kbar with unknown temperature change; (3) near-isothermal decompression from 12 kbar to 2–3 kbar, with some

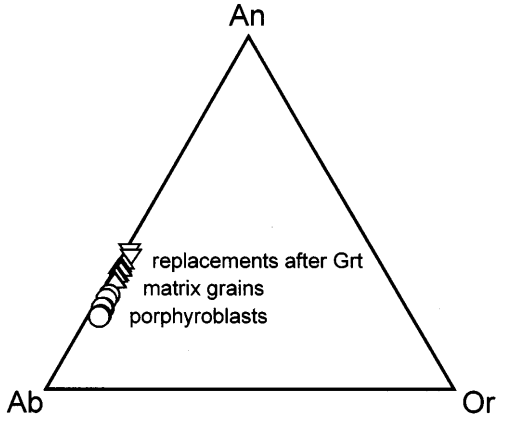

Fig. 10 Ternary anorthite-albite-orthoclase diagram showing the compositional heterogeneity of plagioclase, that bears the highest Ca contents when it replaces garnet

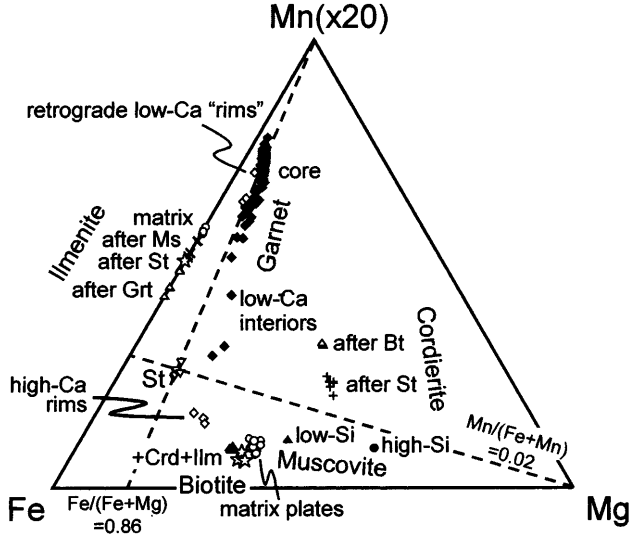

Fig. 11 Ternary Fe-Mg-Mn (atom proportions) diagram showing the compositional heterogeneity of coexisting phases in sample T348, with indication of different textural types of grains

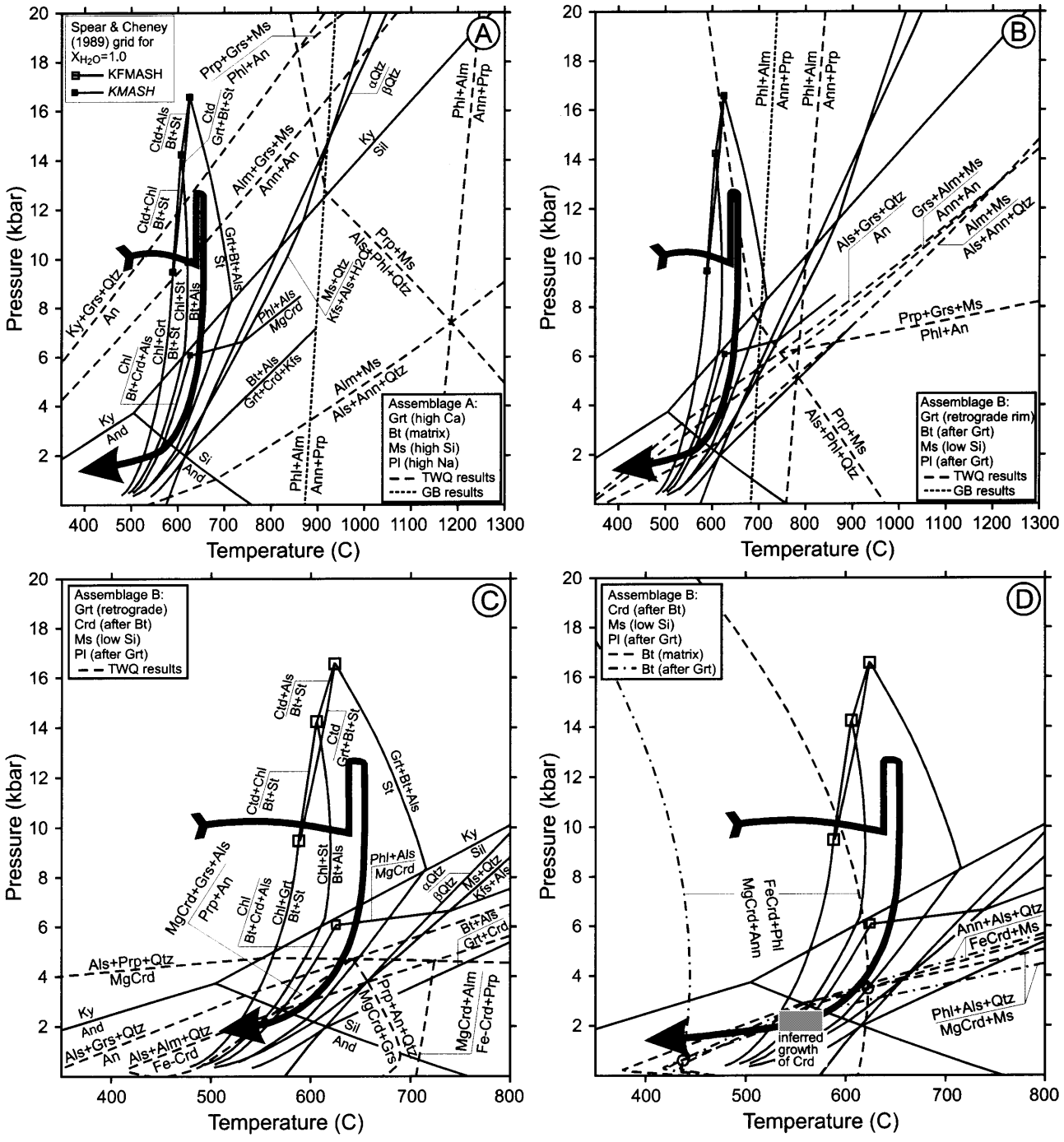

cooling at intermediate to low P ($\Delta T \approx -50$ °C); (4) cooling and termination of metamorphism. In sample T348, the high pressure stage (2) corresponds to the high-Ca garnet rims (i.e. 12 kbar calculated using GASP barometer; Fig. 12A), as well as with the Si, Fe and Mg contents of deformed muscovite plates (6.562, 0.223 and 0.455 atoms per 20 O and 4 OH, respectively), that are very high for muscovite from medium grade metapelites that bear Al-saturated phases (Guidotti 1984). The high-Ti content (up to 0.118 atoms pfu, Fig. 6) of this high-P muscovite also points out that peak-T condition concurred with peak-P.

The results of TWQ software using the product assemblage Crd + Bt(high-Ti) + Pl(high-Ca) + Ms (low-Si) yield temperatures in the range 450–600 °C using Crd-Bt exchange thermometer (Fig. 12D). The intersections of this Crd-Bt thermometer with other reactions with low dP/dT slopes suggest a pressure range of 0.5–3.7 kbar for cordierite growth. Within the framework of the P-T path followed by the Torrox unit, these estimates indicate that cordierite growth took place just at the onset of cooling, near the end of stage 3, at 2–3 kbar and 550–600 °C. This conclusion is supported by the pattern of diffusion zoning that developed

◄

Fig. 12A–D Location of stable solid-solid equilibria calculated with TWQ software (v.2.02) of Berman (1991) and GB software of Holdaway et al. (1997) for sample T348, presented for: **A** the reactant assemblage (high-Ca garnet rims, matrix plates of biotite, relict high-Si muscovite and high-Na plagioclase porphyroblasts, plus Al-silicate), and **B**, **C**, and **D** different combinations of the product assemblage (retrograde garnet "rims", cordierite grown after matrix biotite, high-Ti biotite grown after garnet, low-Si muscovite, and high-Ca plagioclase grown after garnet). The compositions used in the calculations are those of Table 2, and the thermodynamic data of end-members and mixing models used with TWQ are from Berman (1988) and Berman and Aranovich (1996), except for the mixing models of muscovite (Chatterjee and Froese 1975) and plagioclase (Fuhrman and Lindsley 1988). Also plotted are the phase relationships among Grt-St-Als-Crd-Bt-Chl-Cld-Ms-Kfs-Qtz-H_2O in the KFMASH system ($X_{H_2O}^{fluid} = 1$and Fe-Mg ideal mixing) taken from Spear and Cheney (1989), except for the Ky-Sil-And, αQtz-βQtz, Ms + Qtz, and Kfs + Als + H_2O stability fields, that were calculated with TWQ. The *P-T* path is from García-Casco and Torres-Roldán (1996). Lack of equilibrium is indicated by high calculated temperatures using Fe-Mg exchange thermometry. Only the product subassemblage biotite-cordierite (D) yields a reasonable *P-T* window (450–600 °C and 0.5–3.7 kbar)

in garnet and matrix plates of biotite during their replacement, and amounts to considering that sample T348 suffered a pressure drop of ca. 10 kbar for a temperature change not exceeding 100 °C.

Disequilibrium among the solid phases in the studied sample precludes their use to estimate the composition of the coexisting metamorphic fluid during cordierite growth. However, some insights can be gained by examining the equilibrium between graphite and fluid in the C-O-H system following the method of French (1966). Figure 13A represents the type of mixtures expected at 2.5 kbar and 575 °C, which are CH_4-rich at low f_{O_2} and CO_2-rich at high f_{O_2}, and have $X_{H_2O}^{maximum} = 0.815$ for $10^{-21.712}$ bars. The f_{O_2} of the quartz-fayalite-Mag and the Mag-Rt-Ilm buffers calculated for the same *P-T* (after the calibrations of Myers and Eugster 1983, and Ghent 1975) are $10^{-20.336}$ and $10^{-18.331}$ bars, respectively, which are outside the graphite stability limit for this *P-T* ($f_{O_2} = 10^{-20.763}$ bars). This suggests that the value of $10^{-21.712}$ bars for $X_{H_2O}^{max}$ is reasonably low to be consistent with the low values of the Fe_2O_3 component in ilmenite grown at low *P* in sample T348 (Fig. 9). An essentially H_2O rich fluid can also be presumed to have existed at the onset of cordierite growth because dehydration reactions were taking place immediately before cordierite started to grow (reaction 9m, see below). That $X_{H_2O}^{fluid}$ had been close to 0.8 at the time of cordierite growth is also consistent

Fig. 13 A Isothermal and isobaric (575 °C, 2.5 kbar) section of *P-T*-X_i^{fluid}-f_{O_2} space showing the composition of fluid in equilibrium with graphite in the C-O-H system, assuming a real-gas ideal-solution model (i.e. the activity coefficients $\gamma_i = 1$, and the fugacity coefficients $\chi_i \neq 1$, calculated using the expressions of Holland and Powell, 1990 for CO_2 and H_2O, from Ryzhenko and Volkov, 1971 for CH_4, and set to 1 for CO, H_2 and O_2 due to their low abundance in the fluid). Thermodynamic data are from Robie et al. (1978) for CO, and Helgeson et al. (1978) for the rest of species. **B** *P-T* projection of solid-fluid equilibria assuming $X_{H_2O}^{fluid} = 0.8$, as calculated with TWQ software for the assemblage Crd(after matrix biotite) + Bt(after garnet) + Ms(low-Si) + Pl(after garnet) + And. The calculations were performed assuming an H_2O-CO_2 fluid, using the equations of state of Haar et al. (1984) and Kerrick and Jacobs (1981) for the properties of pure H_2O and the mixture, respectively. The properties of the solids are as in Fig. 12. The *circles* correspond to the projection of the pseudoinvariant points for the Fe- and Mg-subsystems at $X_{H_2O}^{fluid} = 0.8$, that plot in the range 550–600 °C and 2–3.5 kbar)

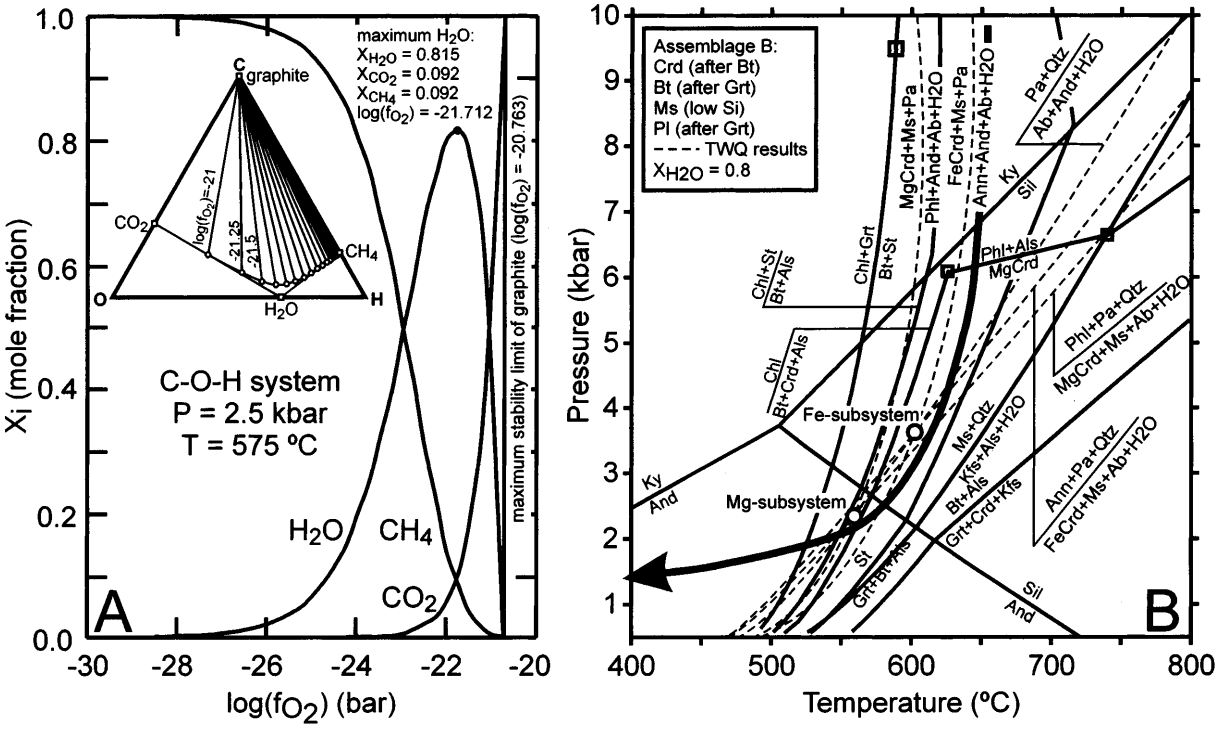

with *P-T* calculations using solid-fluid equilibria. The results of TWQ software using the low-*P* assemblage Crd + Bt + Pl + Ms + And for $X_{H_2O}^{fluid} = 0.8$ yield conditions in the range 550–600 °C and 2–3.5 kbar (Fig. 13B), in good agreement with the calculations using solid-solid equilibria for the same assemblage (Fig. 12D).

Cordierite-forming reactions

At a first glance, the products of garnet and staurolite decomposition would argue in favour of a single reaction process of cordierite growth in sample T348, such as:

$$\text{St} + \text{Grt} + \text{Bt (matrix)} + \text{Ms (high-Si)} + \text{Pl (Na-rich)} + \text{Rt} = \text{Crd} + \text{Bt (high-Ti)} + \text{Ms (low-Si)} + \text{Pl (Ca-rich)} + \text{Ilm} \quad (1t)$$

(t in the reaction label stands for texturally deduced reaction). The compositional heterogeneity of the intervening phases in different reaction sites (i.e. even product cordierite is heterogeneous), however, suggests that the operation of a single bulk reaction (i.e. mass balance) was precluded by diffusion problems. Only local mass balances would be expected appropriately to describe cordierite growth. For example, the following mass balances:

$$0.181\ \text{St} + 4.580\ \text{Bt (matrix)} + 0.149\ \text{Ms (high-Si)} + 0.033\ \text{Pl (high-Na)} + 1.117\ \text{Rt} + 3.047\ \text{Qtz} + 0.199\ \text{H}_2\text{O} = 1.000\ \text{Crd (after St)} + 4.407\ \text{Bt (after St)} + 0.240\ \text{Ms (low-Si)} + 0.115\ \text{Ilm (after St)}, \quad (2c)$$

and

$$2.501\ \text{Grt (high-Ca)} + 2.659\ \text{Bt (matrix)} + 1.232\ \text{Ms (high-Si)} + 4.738\ \text{Pl (high-Na)} + 0.998\ \text{Rt} + 0.840\ \text{H}_2\text{O} = 1.000\ \text{Crd (after Bt)} + 3.962\ \text{Bt (after Grt)} + 5.866\ \text{Pl (high-Ca)} + 0.075\ \text{Ilm (after Grt)} + 1.495\ \text{Qtz}, \quad (3c)$$

adequately describe the incompatibility constraints observed in the textures of staurolite and garnet decomposition, respectively (c in the reaction label stands for reactions calculated in the 10-dimension composition space K_2O-Na_2O-CaO-FeO-MnO-MgO-Al_2O_3-TiO_2-SiO_2-H_2O –KNCFMnMATSH; the calculations were based on SVD techniques, as described by Fisher, 1989, using CSpace software by Torres-Roldán et al. in press). In these reactions the micas and plagioclase are involved as reactant and product phases at a time to account for their compositional shifts and replacement/growth textures. For the conditions in which cordierite was generated in these rocks (ca. 575 °C and 2.5 kbar), cordierite would be expected to have contained between 0.5 and 0.7 moles of H_2O pfu (e.g. McPhail et al. 1990; Skippen and Gunter 1996). Consequently, cordierite was assumed to be hydrated, with 0.7 moles of H_2O per $Si_5Al_4(Fe,Mg,Mn)_2O_{18}$ in the calculations, and H_2O appears as a reactant phase in both reactions. Note that fresh cordierite found within pinite from Crd + Ilm + Qtz replacements after matrix biotite was used to model the garnet decomposition reaction (3c). Given that cordierite is not homogeneous, there is no guarantee that cordierite grown after garnet had this composition, but a very similar reaction would be encountered with any other reliable composition of cordierite because of its tight compositional constraints in terms of Fe-Mg-Mn partitioning and water content.

Predicted phase relations in the KFMASH system

The model pelite KFMASH system is perhaps the most extensively investigated system in the petrologic literature, and the success of the quantitative predictions that are derived from it on the basis of thermodynamic data (i.e. invariant points and linking reactions; e.g. Thompson 1976b; Spear and Cheney 1989; Powell and Holland 1990; Xu et al. 1994) is now widely recognized. Still, some specific points are controversial, and one important example of this concerns the stability of mineral assemblages consisting in cordierite + muscovite + quartz plus garnet or staurolite (thereafter Grt + Crd + Ms and St + Crd + Ms) in medium grade low-*P* metapelites. This topic has been reviewed and discussed by Pattison and Tracy (1991) and Pattison et al. (1996, and D.R.M. Pattison, F.S. Spear and J.T. Cheney, manuscript in preparation).

The stability of Grt + Crd + Ms and St + Crd + Ms assemblages is predicted at low pressure (less than 4–5 kbar) and moderate temperatures (500–650 °C) in most grids published to date since Albee's (1965) grid (e.g. Hess 1969; Thompson 1976b; Kepezhinskas and Khlestov 1977; Harte and Hudson 1979; Hudson 1980; Powell and Holland 1990; Xu et al. 1994). According to these grids, cordierite could be expected to have grown in the Torrox metapelites through one or more of the following reactions, written in the sense of decompression (Fig. 14; absent phases within brackets in place of the equal sign):

$$\text{Bt} + \text{Als} + \text{Qtz} + \text{H}_2\text{O}\ [\text{St,Grt,Chl,Kfs}]\ \text{Crd} + \text{Ms}, \quad (4m)$$

$$\text{Bt} + \text{Als} + \text{Qtz} + \text{H}_2\text{O}\ [\text{Grt,Chl,Kfs}]\ \text{St} + \text{Crd} + \text{Ms}, \quad (5m)$$

$$\text{Bt} + \text{St} + \text{Qtz} + \text{H}_2\text{O}\ [\text{Grt,Als,Chl,Kfs}]\ \text{Crd} + \text{Ms}, \quad (2m)$$

$$\text{St} + \text{Bt} + \text{Qtz} + \text{H}_2\text{O}\ [\text{Als,Chl,Kfs}]\ \text{Grt} + \text{Crd} + \text{Ms}, \quad (1m)$$

$$\text{Grt} + \text{Ms} + \text{Qtz} + \text{H}_2\text{O}\ [\text{St,Als,Chl,Kfs}]\ \text{Crd} + \text{Bt}, \quad (3m)$$

(m in the reaction labels stands for KFMASH-model reactions; hydrated cordierite is assumed). In natural rocks from low-*P* and medium grade contact and regional metamorphic realms, however, assemblages such as Bt + Als + St, Bt + Als + Grt and Bt + Als + Crd are common while Grt + Crd + Ms and St + Crd + Ms are sparse, suggesting that Bt + Als-bearing assemblages are compatible relative to Crd + St- and Crd + Grt-bearing assemblages at medium grade. This led Spear and Cheney (1989), Pattison (1989), and Pattison and Tracy (1991) to construct petrogenetic grids that do not foresee the stable coexistence of Grt + Crd + Ms and St + Crd + Ms at any *P-T* condition in the model pelite KFMASH system

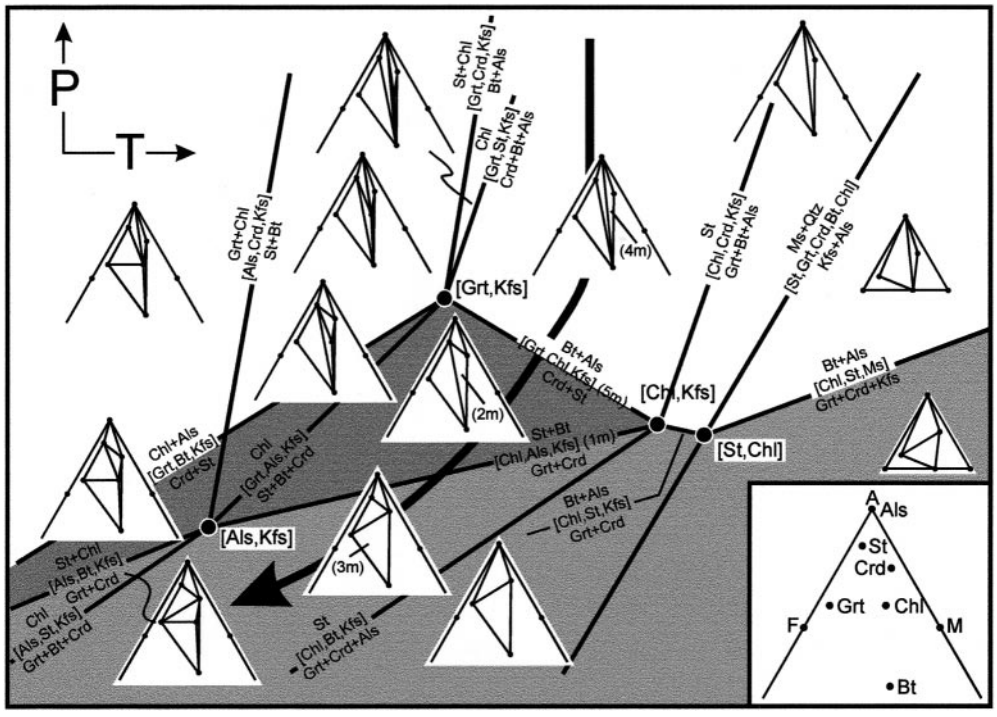

Fig. 14 Schematic representation of the univariant and divariant relationships among the phases St-Grt-Crd-Bt-Als-Chl-Ms-Kfs-Qtz-H_2O in the KFMASH system proposed by Thompson (1976b), as representative of other grids of this type referred to in the text that predict the stable coexistence of St + Crd + Ms (*darker gray area*) and Grt + Crd + Ms(or Kfs) (*lighter gray area*) in Qtz-bearing metapelites. In the reactions, absent phases are *within brackets* and, for the sake of clarity, non-AFM phases are omitted. Note that all types of metapelites of the Torrox unit should have sequentially intersected the univariant reactions (5m) and (1m), for which there are no textural evidence, and reactions (2m) and (3m)

(Fig. 12). Although these authors acknowledge that the effect of extra components, such as Mn and Zn, might help explain some occurrences of these assemblages, they qualify them as apparent, emphasizing their unstable nature in the KFMASH system. In these grids, reactions (5m), (2m), (1m) and (3m) are not predicted (Fig. 12) and cordierite growth upon decompression at medium grade would be expected to take place only through the divariant reaction (4m).

Stable versus metastable processes

Interpreting cordierite growth after garnet and staurolite in the Torrox metapelites hence relies on the type of KFMASH grid used and the effect of extra components. At first glance, the model reactions inferred for sample T348, i.e. (2c), and (3c), are not consistent with the relations predicted by Spear and Cheney's type of grid, but can be identified with the divariant reactions (2m) and (3m) predicted by Albee's type of grid. This overall similarity between observed processes and predictions, in addition to the lack of evidence for reaction (4m), (i.e. the absence of reaction relationships between biotite and andalusite), would thus appear to be more consistent with Albee's type of grid.

Upon closer inspection, however, the agreement with an Albee type of grid is seriously questionable through the analysis of the reactions taking place in sample T348. Reactions (2m) and (3m) are linked by univariant reaction (1m). As long as the reaction processes (2c) and (3c) might represent different parts of the single bulk process like (1t), the latter would be expected to compare well with univariant reaction (1m) which is not possible since in the latter garnet plus cordierite are predicted to grow, while garnet is in fact replaced by cordierite. Furthermore, reactions (2m) and (3m) are only allowed once univariant reaction (5m) is intersected in the sense of decompression (Fig. 14), which again conflicts with textural evidence (andalusite, biotite and cordierite show sharp shared contacts, and staurolite is replaced by cordierite). That is, using Albee's type of grid one is forced to conclude that the higher-variance reactions (2m) and (3m) were operative and produced noticeable changes in textures and mineral abundances, but that the limiting lower-variance reactions (5m) and (1m), that should also have been intersected, did not. This is something difficult to envisage, even if other factors complicate the predictions of this type of KFMASH grid. The presence of extra components would merely increase the variance of the reactions and hence cannot be raised as a factor controlling what reactions were operational. The availability of H_2O, on the other hand, is a control for the extent of reaction, but not for the reactions intersected since all the possible reactions involved, either actually occurring (2m) and (3m), or predicted (4m), (5m) and (1m) bear H_2O as a reactant.

A number of factors could have contributed to avoid the intersection of reactions (5m) and (1m), including a different shape of the *P-T* path, a more restricted *P-T* range of stability of Crd + Ms + Qtz ± St ± Grt assemblages, and even the complete instability of Crd + Ms + Qtz ± St ± Grt assemblages. However, in any of these cases the reaction processes (2c) and (3c) should not have been operative because the multicomponent equivalents of reactions (2m) and (3m) could not have been intersected. This paradox leads finally to the consideration that observed reaction processes (2c) and (3c) have operated metastably, in which case there is no need for the stability of the multicomponent equivalents of reactions (5m) and (1m), in accordance with the predictions of Spear and Cheney's type of grid. In this scenario, reaction processes (2c) and (3c) could have operated within the stability field of Crd + And + Bt instead of the multicomponent equivalent of the predicted reaction (4m), requiring only that both garnet and staurolite persisted at low-*P* after decompression. The relict character of garnet and staurolite is in good agreement with the textural and compositional features as discussed above, and is otherwise consistent with a similar conclusion in the cordierite-lacking metapelites of the Torrox unit (García-Casco and Torres-Roldán 1996). D.R.M. Pattison (written communication and manuscript in preparation) noted that cooling might be necessary after the Grt + St event to preserve these phases metastably during an hypothetical second thermal pulse that would have produced And + Bt ± Crd assemblages at low *P* (cf. Pattison and Harte 1991). This possibility, however, does not fit the diffusional profiles that developed in garnet and biotite, which indicate that cordierite growth took place along with cooling + decompression, nor with the occurrence of immediate fast cooling as required in order to preserve diffusive zoning in biotite.

Model reaction history

To discuss the operation of reactions (2m) and (3m) as metastable processes instead of (4m), it is necessary to analyse in detail the phase relations predicted within Spear and Cheney's type of grid for a decompression path. The calculations have been accomplished by means of the Gibbs method (Spear et al. 1982) as managed by program GIBBS (Spear and Menard 1989). In the calculations we followed the procedure of Spear and Cheney (1989) and assumed the extrapolation of available thermodynamic and experimental data and inferences made by these authors. Consequently, we used the *P-T-X* relations of the KFMASH invariant points given by Spear and Cheney in their Table 4 as reference points. Yet, these authors did not give any *P-T-X* reference point involving cordierite, so we had to calculate two additional reference points necessary to derive the relations involving this phase. The *P-T-X* conditions of these reference points correspond to (#1) P = 2000 bars, T = 605 °C for the univariant assemblage Ms-Qtz-Kfs-And-H_2O, and (#2) P = 2000 bars, T = 615 °C for the univariant assemblage Grt(X_{Fe} = 0.8755)-Crd(X_{Fe} = 0.37)-Bt(X_{Fe} = 0.5747) -Sil-Kfs-Qtz-H_2O (using a hydrated cordierite with 0.7 moles of H_2O per formula unit). While the P and T conditions of these reference points were extracted visually from the Spear and Cheney (1989) grid, the X conditions of reference point (#2) were calculated by solving first for biotite and garnet composition at the reference *P-T* through the KFMASH-divariant assemblage:

$$\text{Bt} + \text{Als} + \text{Qtz} \; [\text{Chl,St,Crd,Ms}] \; \text{Grt} + \text{Kfs} + \text{H}_2\text{O}, \qquad (6\text{m})$$

and then solving for cordierite composition at this reference *P-T-X* condition through the exchange reaction $FeMg_{-1}^{Grt} = FeMg_{-1}^{Crd}$ using the enthalpy, entropy and volume of reaction given by Spear and Cheney (1989) in their Table 3, and the C_P data of the end-members given in their Table 1.

Fig. 15 shows the phase relations expected for the decompression path of the Torrox metapelites (Fig. 12), characterized by an isothermal section (650 °C, from 12 to 6 kbar), followed by decompression plus cooling with increasing $\partial T/\partial P$ slopes from 6 to 1 kbar. This pseudobinary section of P-T-X_{Fe}^{solids}-$X_{H_2O}^{fluid}$ space in the KFMAS-H_2O-CO_2 system assumes $X_{H_2O}^{fluid} = 0.8$, although this restriction is relaxed at higher P in Fig. 17, calculated for sample T348 within the KNCFMnMA-TiS-H_2O-CO_2 system. Note that the calculated sections avoid the intersection of the maximum stability limits of St + Qtz + Ms and Ms + Qtz at low P, as there is no textural evidence for the breakdown of staurolite and muscovite at low P through:

$$\text{St} + \text{Ms} + \text{Qtz} \; [\text{Chl,Crd,Kfs}] \; \text{Bt} + \text{Grt} + \text{Sil (or And)} + \text{H}_2\text{O} \qquad (7\text{m})$$

$$\text{Ms} + \text{Qtz} \; [\text{St,Grt,Crd,Chl}] \; \text{Kfs} + \text{Sil (or And)} + \text{H}_2\text{O}. \qquad (8\text{m})$$

A similar reaction sequence is predicted before cordierite growth for cordierite-bearing and cordierite-lacking rocks (Fig. 15), contrasted only in terms of differences in the Fe/(Fe + Mg) ratio of bulk compositions. Reactions are triggered along the decompression path by the shifts of the Fe/(Fe + Mg) ratios of coexisting phases towards Fe-richer compositions (Figs. 15 and 17; García-Casco and Torres-Roldán 1996). At low P, cordierite growth would only be expected in rocks with lower Fe/(Fe + Mg) ratios, through reaction (4m), when these compositions intersect the And + Bt tie-line limiting the Crd + And + Bt field. In the case of the Torrox metapelites, however, the relict persistence of staurolite and garnet outside their stable P-T-X_{Fe} ranges (i.e. the [Grt,Crd,Chl,Kfs] and [Crd,Als,Chl,Kfs] loops in Figs. 15 and 17) conceivably conditioned cordierite growth to proceed instead through the metastable multicomponent equivalents of reactions (2m) and (3m). That is, within this model system, cordierite grew as a response to equilibrium requirements, but proceeded through non-equilibrium reaction pathways as the most efficient way to

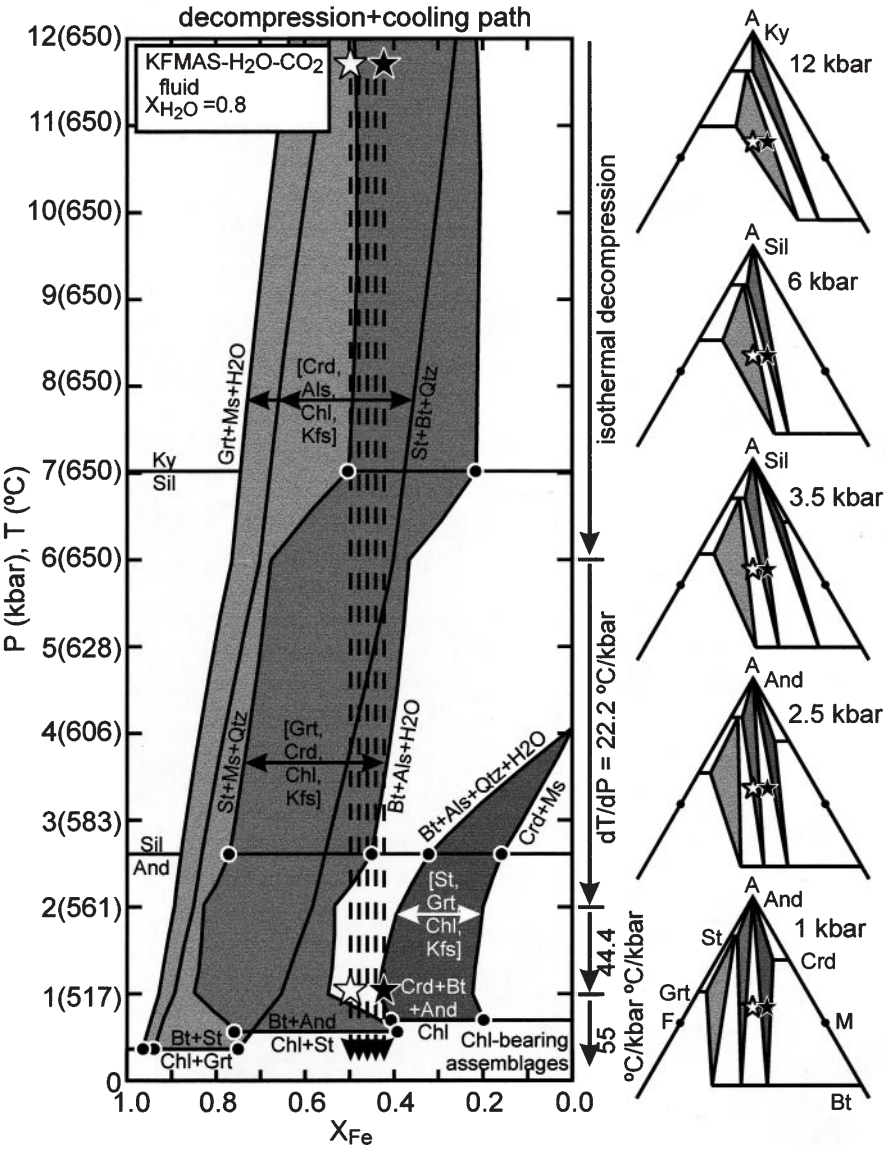

Fig. 15 Pseudobinary P-X_{Fe}^{solids} non-isothermal section in the KFMAS-H_2O-CO_2 system, calculated using the program GIBBS (Spear and Menard 1989) with the thermodynamic database of Berman (1988), as modified by Spear and Cheney (1989), ideal mixing models for the solid solutions, and the CO_2-H_2O mixing model of Kerrick and Jacobs (1981) for $X_{H_2O}^{fluid} = 0.8$. The section follows a P-T path characterized by isothermal decompression (16–6 kbar at 650 °C) and cooling + decompression (6–1 kbar), with a dT/dP slope increasing as P decreases, from 22 °C/kbar, through 44 °C/kbar to 55 °C/kbar, as appropriate for the Torrox unit (Fig. 12). Note that the expected AFM assemblages and reaction sequence developing upon decompression are similar for Fe-richer (*empty star*) and Mg-richer bulk compositions (*filled star*), except at low P, where the latter would be expected to develop cordierite through the stable reaction (4m-And) [St,Grt,Chl,Kfs]. This bulk composition effect further helps to explain that cordierite is only locally developed in the Torrox metapelites, irrespective of their metamorphic grade

minimize the Gibbs free energy of a system already largely deviated from equilibrium. This explanation satisfies the observed reaction textures, the lack of textural evidence for Bt + Als reaction, the disequilibrium Fe-Mg partitioning among the coexisting phases, and the fact that cordierite-bearing assemblages are found only locally in rocks of appropriate Mg-richer composition, while most rocks display And + Bt as the stable assemblage at low P (note that Albee's type of grid predicts that cordierite should have been produced in most metapelites of the Torrox unit, and not just in some rocks).

Effect of extra components

It could be argued that the effect of extra components in the solids, particularly Zn and Mn, and/or the buffering of fluid composition, could help to explain the operation of reactions (2c) and (3c) as stable processes, the opposite to our conclusion of metastable progress. To analyse these effects, we have evaluated the modification of the stability limits of St + Bt + And and Crd + Bt + And assemblages due to CO_2 dissolved in the fluid, Zn in staurolite, and Mn in cordierite, using the Gibbs method as above, with the thermodynamic data of Wang and Spear (1991) for Zn-staurolite. The results are illustrated for 2.5 kbar and 575 °C in Fig. 16, where it can be appreciated that a decrease in $X_{H_2O}^{fluid}$ shrinks, and an increase in X_{Zn}^{St} and/or X_{Mn}^{Crd} expands, the stability of St + Bt + And and Crd + Bt + And assemblages. The latter effects represent maximum isothermal-isobaric shifts of the reactions:

St + Ms + Qtz [Grt,Crd,Chl,Kfs] Bt + And + H_2O (9m-And)

and (4m) [St,Grt,Chl,Kfs] since we assumed that Zn and Mn are incorporated only in staurolite and cordierite, respectively. This approximation is appropriate for Zn, but not for Mn that could be present in biotite, stauro-

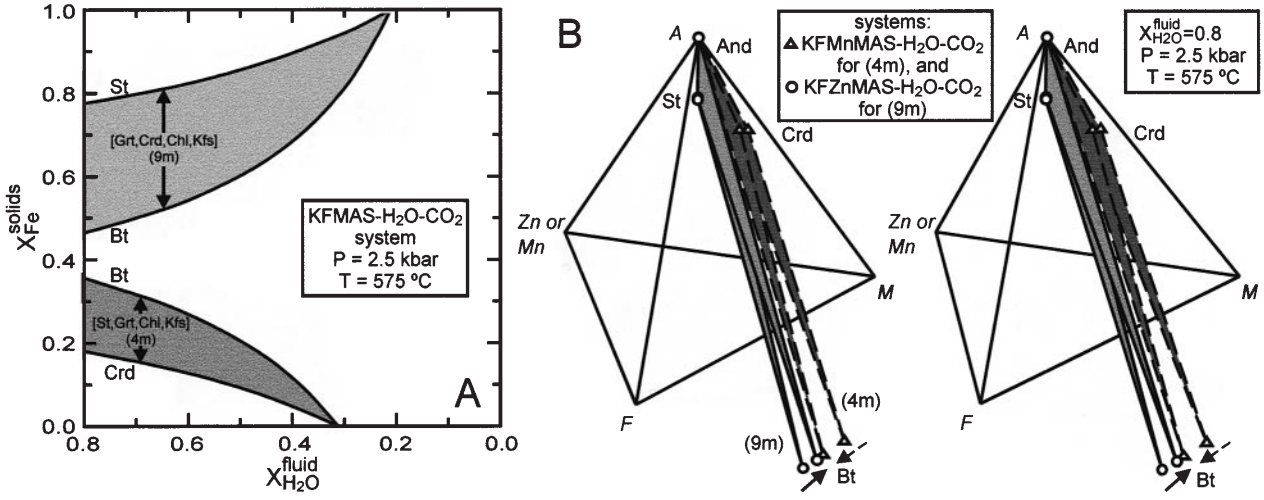

Fig. 16 **A** Isothermal and isobaric (575 °C, 2.5 kbar) section of *P-T-*X_{Fe}^{solids} $X_{H_2O}^{fluid}$ space in the KFMAS-H_2O-CO_2 system, showing that the stability of St + Bt + And and Crd + Bt + And assemblages ([Grt,Crd,Chl,Kfs] (9m) and [St,Grt,Chl,Kfs] (4m) loops, respectively) shrink at low $X_{H_2O}^{fluid}$. **B** Isothermal and isobaric (575 °C, 2.5 kbar) AFM-Mn-or-Zn tetrahedron showing the expansion of St + Bt + And and Crd + Bt + And assemblages due to increasing Zn and Mn contents in staurolite and cordierite, respectively, in the KFMZnAS-H_2O-CO_2 and KFMMnAS-H_2O-CO_2 systems for $X_{H_2O}^{fluid} = 0.8$. This effect implies the overlapping of St + Bt + And and Crd + Bt + And assemblages in the KFMMnZnAS-H_2O-CO_2 system, since X_{Fe}^{solid} decreases and increases, respectively, in both assemblages as staurolite and cordierite get richer in Zn and Mn, respectively (*arrows*). This would allow for the stability of St + Crd assemblages and the multicomponent equivalents of reactions (5m) and (2m) in Ms- and Qtz-bearing rocks rich in Mn and/or Zn

lite, and andalusite (the presence of Mn in other phases would diminish this effect; see Spear and Cheney 1989, for a similar effect of Mn in Grt-bearing assemblages).

The effect of Zn and Mn components anticipates that St + Bt + And and Crd + Bt + And assemblages might overlap in the KFMZnMnAS-H_2O-CO_2 system, allowing for the stable coexistence of St + Crd + Bt + And in Zn- and/or Mn-rich metamorphic rocks, as noted by Pattison and Tracy (1991), Dymoke and Sandiford (1992) and Pattison et al. (1996), and for the operation of reaction (5m). In the Torrox metapelites, however, any such overlap is not regarded as feasible given that: (1) there is no textural evidence for reaction (5m); (2) Zn/(Zn + Fe + Mg) is less than 0.05 in staurolite and Mn/(Mn + Fe + Mg) less than 0.02 in cordierite, staurolite, biotite and garnet rims (see Fig. 11). To these one might add the counterbalancing effect of a reduced $X_{H_2O}^{fluid}$ (≤0.8), as well as the predicted effect of other components in the solids, such as Ti, which would be expected to moderate the effects of Mn and Zn, since Ti is known to be partitioned strongly into biotite relative to staurolite, cordierite, Al-silicate, and muscovite. The lack of thermodynamic data for Ti-bearing components in biotite hampers a formal estimation of this effect, but it could be significant in these Ti-saturated systems with ilmenite or rutile.

The above arguments also apply to the effect of extra components in garnet-bearing assemblages, and suggest that neither staurolite nor garnet ever coexisted in equilibrium with cordierite in the Torrox metapelites. Again, this indicates that the stable reaction that could have been expected to produce cordierite should have been a multicomponent equivalent of the divariant reaction (4m), and that reactions (2c) and (3c) operated as metastable processes under conditions that were largely deviated from equilibrium. Assuming this, a theoretical equilibrium reaction path undergoing decompression (+ cooling at low *P*) is presented in Fig. 17 for sample T348 in the system KNCFMnMATiS-H_2O-CO_2. In these *P-T-V*(volume)^{solids}-X_{Fe}^{solids}-X_{Mn}^{solids}-$X_{H_2O}^{fluid}$ pseudosections it was also assumed that kyanite, rutile, garnet and staurolite should have been consumed sequentially upon decompression, as predicted in Fig. 15 (see also García-Casco and Torres-Roldán 1996). Figure 17 shows that the stable reaction pathway should have consisted of the multicomponent equivalents of reactions:

Grt + Ms [St,Crd,Chl,Kfs] Bt + Ky + Qtz, (10m-Ky)

Bt + Grt + Ky + H_2O [Crd,Chl,Kfs] St + Ms + Qtz, (7m-Ky)

Grt + Ms + H_2O [Crd,Als,Chl,Kfs] St + Bt + Qtz, (11m)

St + Ms + Qtz [Grt,Crd,Chl,Kfs] Bt + Fib + H_2O, (9m-Sil)

Bt + And + Qtz + H_2O [St,Grt,Chl,Kfs] Crd + Ms (4m-And)

(triggered in the indicated sequence), which would have conditioned assemblages to change from pre-D_2 Grt + Ky + Bt (equilibrated at peak pressure conditions), through syn-D_2 St + Grt + Bt and St + Fib + Bt to post-D_3 Crd + And + Bt. Note that, although sample T348 lacks kyanite, many samples of the Torrox unit (either bearing or lacking cordierite) still bear relicts of this phase as well as textural evidence for reactions (10m-Ky) and (7m-Ky) (García-Casco and Torres-Roldán 1996).

The phase relationships depicted in Figs. 15 and 17 do also help to interpret other features of the studied rock, in a context where pressure and temperature (at low *P*) were rapidly changing. The predicted increase in

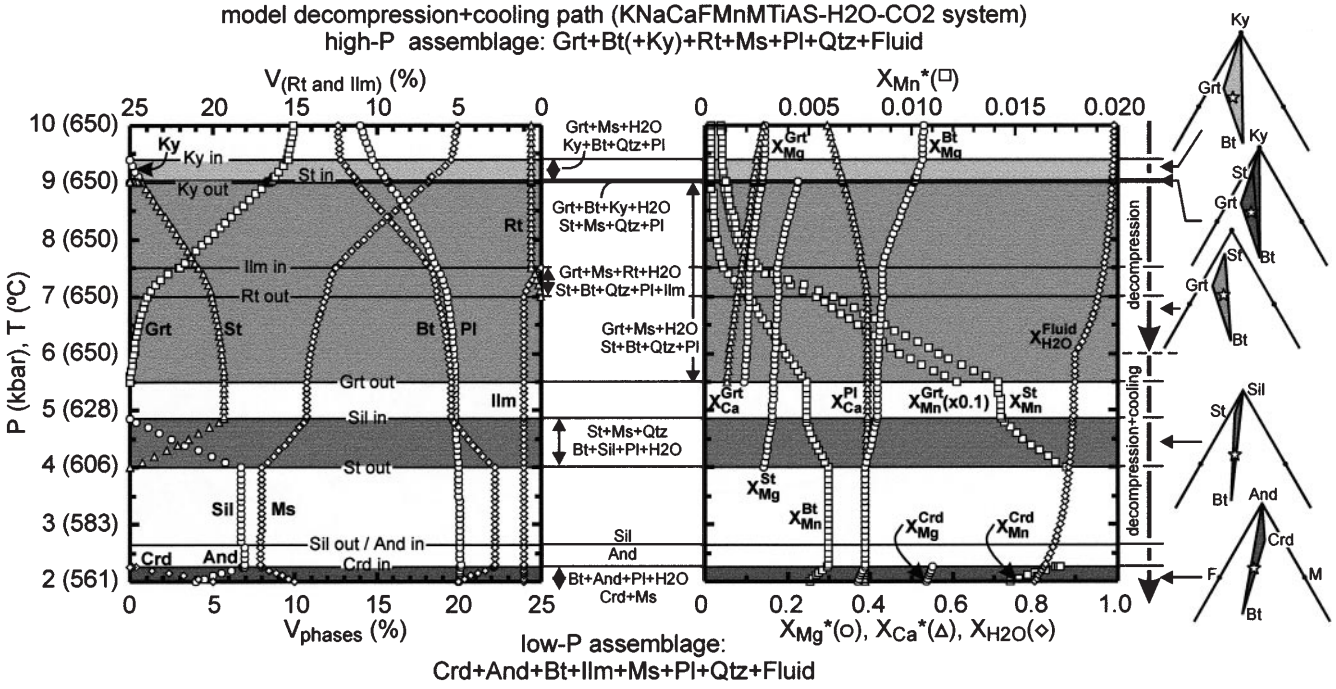

Fig. 17 *P-T-V*(volume)^{solids}-X_{Mg}^{solid}-X_{Mn}^{solid}-X_{Ca}^{solid}-$X_{H_2O}^{fluid}$ pseudosections and AFM diagrams showing the theoretical (i.e. equilibrium) reaction path appropriate for sample T348 in the system K_2O-Na_2O-CaO-FeO-MnO-MgO-Al_2O_3-TiO_2-SiO_2-H_2O-CO_2 undergoing the same model decompression + cooling *P-T* path as in Fig. 15. The diagrams were constructed using the Gibbs method through a *backwards* procedure, i.e. starting the calculations at low *P* (2 kbar and 561.2 °C), with the composition of the phases from the low-*P* assemblage Qtz-Ms-Pl-Ilm-And-Bt-Crd-H_2O taken from sample T348 (Table 2) assuming that fluid fractionates (i.e. $X_{H_2O} = 0$) and that staurolite, garnet (compositions in Table 2), rutile and kyanite joined the evolving (i.e. up pressure) assemblages at 4, 5.5, 7 kbar and 9 kbar, respectively. Note that the latter assumptions make the multicomponent equivalent of reaction (4m-And) stable and, consequently, responsible for the production of cordierite. All the multivariant reactions are written with reactants and products at higher and lower *P*, respectively, and their limits labelled with the key phases that enter/exit the evolving assemblages. The thermodynamic data used in the calculations are those of Spear and Cheney (1989), except for ilmenite and rutile that were taken from Berman (1988)

Fe/(Fe + Mg) ratio of garnet upon decompression is in accordance with the increasing Fe/(Fe + Mg) ratio of the low-Ca garnet interiors modified by diffusion at the time of cordierite replacement (Fig. 4). The predicted increase in the Fe/(Fe + Mg) ratio of staurolite explains the reverse Mg-Fe partitioning between this phase and the relict high-Ca garnet rims (Fig. 11). The anomalous Mn partition among high-Ca garnet rims and staurolite ($X_{Mn}^{St} > X_{Mn}^{Grt(high-Ca\ rim)}$), and the normal Mn partition among retrograde garnet and staurolite and cordierite, also find explanation in that X_{Mn} in garnet equilibrated at high *P* must be low, and X_{Mn} should increase in staurolite and garnet upon decompression. On the other hand, the high Fe/(Fe + Mg) ratio of matrix biotite, similar to that of newly formed replacement biotites (Fig. 10), indicates that all types of biotite acquired their present composition at relatively low *P*, thus giving place to odd biotite-garnet thermometric results (Fig. 12). Increase of X_{Fe} across the late diffusive rims that developed in these biotites during cordierite growth (Fig. 8) is further consistent with onset of cooling (and continued decompression). To be noted, also, is that the increase in the Fe/(Fe + Mg) ratio of muscovite as Si decreases (Fig. 6) is in accordance with the predicted increase in the Fe/(Fe + Mg) ratio of all the coexisting Fe-Mg phases as pressure decreases. Lastly, the trend towards higher Ca contents in growing plagioclase upon decompression is consistent with the observed higher X_{Ca} of late plagioclase (both in the matrix and the replacements, Fig. 10).

Discussion and implications

Implications for *P-T* grids

Given the present limitations of experimental work and the uncertainties of the thermodynamic properties of the phases, the best way to test the applicability of *P-T-X* grids is the comparison of their theoretical predictions with actual metamorphic reaction histories, as inferred from textures and phase relations in natural rocks. In most cases, however, only natural observations related to increasing grade have been used for this purpose (e.g. Pattison and Tracy 1991) or, conversely, the grids are used to confirm observations in prograde sequences. Using metamorphic rocks where the main changes are related to pressure is more challenging in that one has to deal with complex phase relations and disequilibrium within single samples, but has distinct advantages that may help discriminating among different grids and their

respective assumptions and theoretical approaches. Our analysis of cordierite-forming reactions in the Torrox metapelites is particularly relevant for the controversial stability of Crd + St + Ms + Qtz and Crd + Grt + Ms + Qtz assemblages. In this regard, we have shown that, while KFMASH reactions (2m) and (3m) compare well with the observed reaction processes, a variety of arguments pertaining to the recorded textures, phase relationships and field distribution of cordierite-bearing rocks from the Torrox unit militate against the type of grid that predicts reactions (2m) and (3m) and, consequently, the existence of a wide *P-T* range of stable coexistence of Crd + Ms + Qtz ± Grt ± St in medium grade, low-*P* metapelites (Pattison and Tracy 1991; Pattison et al. 1996 and written communication). This would be in favour of grids that do not predict the stable coexistence of these assemblages, at least in normal metapelites (i.e. Mn and/or Zn-poor) and particularly under reduced $X_{H_2O}^{fluid}$. Still, the complexity of our rocks does not allow excluding the possibility of a limited *P-T* range of stability of Crd + St + Ms + Qtz and/or Crd + Grt + Ms + Qtz assemblages in normal metapelites equilibrated under high $X_{H_2O}^{fluid}$, and this is indeed pointed out by some of the occurrences of these assemblages in nature where, contrary to our case, equilibrium is suspected (e.g. Dymoke and Sandiford 1992; Reinhardt and Kleemann 1994; Alías 1995).

Implications for the development of extensional collapse of the Betic-Rif Belt

The high degree of preservation of decompression-related disequilibrium features in sample T348, including that of fine diffusive zoning in biotite, indicates termination of metamorphism through rapid cooling. Similar pervasive disequilibrium is a general feature of other rocks in the area (García-Casco et al. 1993; García-Casco and Torres-Roldán 1996), and may be correlated with current estimates of cooling rates as summarized in the introduction. The triggering of cordierite-forming reactions, on the other hand, implies that the onset of cooling of the Torrox rocks took place at low pressure (less than about 3 kbar), in the lowest range of previous estimates (e.g. Zeck et al. 1989). While still consistent with the occurrence of high uplift rates during cooling (see Monié et al. 1994 and references therein for additional details), the evidence for a delayed thermal relaxation and for the continuous overstepping of equilibrium boundaries during the petrologic development of the Torrox rocks (see García-Casco et al. 1993 and García-Casco and Torres-Roldán 1996) strongly suggests that comparable or even higher uplift rates have also been operational in the pre-cooling stage, and that decompression has been continuous from peak pressure down to final uplift during extension. As a corollary, the onset of extension would not be expected to be much earlier than the onset of cooling, which agrees with thermal modelling by Platt et al. (1998), where the start of decompression is estimated at about 27 Ma and results in decompression rates of 4–5 km/Ma for the main decompression stage.

Direct dating of the beginning of extensional collapse is not yet well constrained, the more plausible estimate being that of Monié et al. (1991) that postulated onset of extension about 25 Ma ago based on the $^{40}Ar/^{39}Ar$ age of a high-*P*/low-*T* phengite from the Trevenque unit. Tubía et al. (1997) have proposed a 20 ± 2.0 Ma for peak-*P* conditions in eclogite pods of the Ojén unit (SHRIMP age of rims of zircons; Sánchez-Rodríguez et al. 1996), implying an exhumation rate of ≥17 km/Ma. This large exhumation rate might be overestimated, however, if the zircon-based age also reflects the onset of cooling at lower *P* as suggested by the overlap with other cooling ages in the area. All observations are nonetheless consistent with a view of extensional collapse of the Betic-Rif Belt as a single event during which very fast and continued uplift could have taken place in a few Ma during the Oligocene–Miocene transition. The above conclusion is at variance with the proposal by Balanyá et al. (1997) and Azañón et al. (1998) that alternating contractional and extensional events took place before cooling and termination of metamorphism. The occurrence of any significant discontinuity in the process of extension, however, would be expected to have left a record of re-equilibration of assemblages at intermediate pressures (which is not observed in the Torrox unit) and, as noted by Platt et al. (1998), would otherwise be difficult to reconcile with the thermochronological constraints on the metamorphic history of these rocks.

Acknowledgements Thanks are given to David R.M. Pattison for his thorough and constructive review, and for providing us with a preprint of a paper in preparation by himself, F. Spear and J. Cheney that discusses Crd + St + Ms stability. Financial support for this work was provided by the Spanish DGES (Project PB96-1426) and the Junta de Andalucía (Research Group RNM 268).

References

Albee AL (1965) A petrogenetic grid for the Fe-Mg silicates of pelitic schists. Am J Sci 263: 512–536

Alías G (1995) Hercynian metamorphism in metapelites from the western sector of the Aston and Hospitalet massives (Central Pyrenees) (in Catalan, unpublished) PhD thesis, Barcelona Univ

Andriessen PAM, Zeck HP (1996) Fission-track constraints on timing of Alpine nappe emplacement and rates of cooling and exhumation, Torrox area, Betic Cordilleras, S. Spain. Chem Geol 131: 199–206

Azañón JM, García-Dueñas V, Goffé B (1998) Exhumation of high-pressure metapelites and coeval crustal extension in the Alpujarride complex (Betic Cordillera). Tectonophysics 285: 231–252

Bakker HE, De Jong K, Helmers H, Biermann C (1989) The geodynamic evolution of the Internal Zone of the Betic Cordilleras (south-east Spain): a model based on structural analysis and geothermobarometry. J Metamorphic Geol 7: 359–381

Balanyá JC, García-Dueñas V, Azañón JM (1997) Alternating contractional and extensional events in the Alpujárride nappes of the Alboran Domain (Betics, Gibraltar Arc). Tectonics 16: 226–238

Berman RG (1988) Internally consistent thermodynamic data for stoichiometric minerals in the system Na_2O-K_2O-CaO-MgO-FeO-Fe_2O_3-Al_2O_3-SiO_2-TiO_2-H_2O-CO_2. J Petrol 29: 445–522

Berman RG (1991) Thermobarometry using multiequilibrium calculations: a new technique with petrologic applications. Can Mineral 29: 833–855

Berman RG, Aranovich L Ya (1996) Optimized standard state and mixing properties of minerals. I. Model calibration for olivine, orthopyroxene, cordierite, garnet, and ilmenite in the system FeO-MgO-CaO-Al_2O_3-TiO_2-SiO_2. Contrib Mineral Petrol 126: 1–24

Boulin J (1970) Etudes géologiques dans les zones internes des Cordillères Bétiques de Málaga a Motril (Espagne Meridionale). Thesis, Univ Paris, Ann Hebert Haug 10

Chatterjee ND, Froese EF (1975) A thermodynamic study of the pseudobinary join muscovite-paragonite in the system KAlSi_3O_8-$NaAlSi_3O_8$-Al_2O_3-SiO_2-H_2O. Am Mineral 60: 985–993

Couturié JP, Kornprobst J (1977) Une interprétation geodynamique de l'evolution polyphasée des assemblages des granulites dans les chaînes bético-rifaines et le Massif central français. C R Somm Seances Soc Geol Fr 5: 289–291

Cuevas J, Navarro-Vilá F, Tubía JM (1989) Interprétation des cisaillements ductiles vers le NE dans les gneiss de Torrox (Complexe Alpujarride, Cordillères Bétiques). Geodin Acta 3: 107–116

Docherty C, Banda E (1995) Evidence for the eastward migration of the Alboran Sea based on regional subsidence analysis: a case for basin formation by delamination of the subcrustal lithosphere? Tectonics 14: 804–818

Dowty E (1980) Crystal-chemical factors affecting the mobility of ions in minerals. Am Mineral 65: 174–182

Dymoke P, Sandiford M (1992) Phase relationships in Buchan facies series pelitic assemblages: calculations with application to andalusite-staurolite parageneses in the Mount lofty Ranges, South Australia. Contrib Mineral Petrol 110: 121–132

Elorza JJ, Garcia-Dueñas V (1981) Hoja y memoria explicativa de la Hoja no 1054 (Vélez-Málaga) del Mapa Geológico de España, escala 1:50000 (Ser Magna). Inst Geol Min Esp, Madrid

Elorza JJ, Garcia-Dueñas V, Martín L, Matos J (1979) Hoja y memoria explicativa de la Hoja no 1040 (Zafarraya) del Mapa Geológico de España, escala 1:50000 (Ser Magna). Inst Geol Min Esp, Madrid

Feenstra A, Engi M (1998) An experimental study of the Fe-Mn exchange between garnet and ilmenite. Contrib Mineral Petrol 131: 379–392

Fisher GW (1989) Matrix analysis of metamorphic mineral assemblages and reactions. Contrib Mineral Petrol 102: 69–77

Florence FT, Spear FS (1991) Effects of diffusional modification of garnet growth zoning on *P-T* path calculations. Contrib Mineral Petrol 107: 487–500

French BM (1966) Some geological applications of equilibrium between graphite and a C-O-H gas phase at high temperatures and pressures. Rev Geophys 4: 233–251

Fuhrman ML, Lindsley DH (1988) Ternary-feldspar modeling and thermometry. Am Mineral 73: 201–216

Ganguly J, Saxena SK (1987) Mixtures and mineral reactions. Springer-Verlag, Berlin Heidelberg New York Tokyo

García-Casco A, Torres-Roldán RL (1996) Disequilibrium induced by fast decompression in St-Bt-Grt-Ky-Sil-And metapelites from the Betic Belt (southern Spain). J Petrol 37: 2107–1239

García-Casco A, Sánchez-Navas A, Torres-Roldán RL (1993) Disequilibrium decomposition and breakdown of muscovite in high *P-T* gneisses, Betic alpine belt (southern Spain). Am Mineral 78: 158–177

García-Dueñas V, Balanyá JC, Martínez-Martínez JM (1992) Miocene extensional detachments in the outcropping basement of the northern Alboran Basin (Betics) and their tectonic implications. Geo-Mar Lett 12: 88–95

Gessmann CK, Spiering B, Raith M (1997) Experimental study of the Fe-Mg exchange between garnet and biotite: constraints on the mixing behavior and analysis of the cation-exchange mechanism. Am Mineral 82: 1225–1240

Ghent ED (1975) Temperature, pressure, and mixed-volatile equilibria attending metamorphism of staurolite-kyanite-bearing assemblages, Esplanade Range, British Columbia. Geol Soc Am Bull 86: 1654–1660

Guidotti CV (1984) Micas in metamorphic rocks. In: Bailey S.W. (ed) (Micas Reviews in Mineralogy, 13) Mineral Soc Am, Washington, DC, pp 357–468

Guidotti CV, Dyar MD (1991) Ferric iron in metamorphic biotite and its petrologic and crystallochemical implications. Am Mineral 76: 161–175

Guidotti CV, Cheney JT, Guggenheim S (1977) Distribution of titanium between coexisting muscovite and biotite in pelitic schists from northwestern Maine. Am Mineral 62: 438–448

Haar L, Gallagher JS, Kell GS (1984) NBS/NRC steam tables: thermodynamic and transport properties and computer program for vapor and liquid states of water in SI units. Hemisphere Publishing Corp., Washington, DC

Harte B, Hudson NFC (1979) Pelite facies series and the temperature and pressures of Dalradian metamorphism in eastern Scotland. In: Harris AL, Holland CH, Leake BE (eds) The Caledonides of the British Isles: reviewed. Geol Soc London Spec Publ 8, pp 323–336

Helgeson HC, Delany JM, Nesbitt HW, Bird DK (1978) Summary and critique of the thermodynamic properties of rock-forming minerals. Am J Sci 278-A: 1–229

Hess PC (1969) The metamorphic paragenesis of cordierite in pelitic rocks. Contrib Mineral Petrol 24: 191–207

Holdaway MJ, Dutrow BL, Shore P (1986) A model for the crystal chemistry of staurolite. Am Mineral 71: 1142–1159

Holdaway MJ, Mukhopadhyay B, Dyar MD, Guidotti CV, Dutrow BL (1997) Garnet-biotite geothermometry revised: new Margules parameters and a natural specimen data set from Maine. Am Mineral 82: 582–595

Holland TJB Powell R (1990) An enlarged and updated internally consistent thermodynamic data set with uncertainties and correlations: the system K_2O-Na_2O-CaO-MgO-MnO-FeO-Fe_2O_3-Al_2O_3-TiO_2-SiO_2-C-H_2-O_2. J Metamorphic Geol 8: 89–124

Hudson NFC (1980) Regional metamorphism of some Dalradian pelites in the Buchan area, N.E. Scotland. Contrib Mineral Petrol 73: 39–51

Kepezhinskas KB, Khlestov VV (1977) The petrogenetic grid and subfacies for middle temperature metapelites. J Petrol 18: 114–143

Kerrick DM (1990) The Al_2SiO_5 polymorphs. (Reviews in Mineralogy, 22) Mineral Soc Am, Washington, DC

Kerrick DM, Jacobs GK (1981) A modified Redlich-Kwong equation for H_2O, CO_2, and H_2O-CO_2 mixtures at elevated pressures and temperatures. Am J Sci 281: 735–767

Kretz R (1983) Symbols for rock-forming minerals. Am Mineral 68: 277–279

Lonergan L, White N (1997) Origin of the Betic-Rif mountain belt. Tectonics 16: 504–522

Loomis TP (1972a) Contact metamorphism of pelitic rock by the Ronda ultramafic intrusion, southern Spain. Geol Soc Am Bull 83: 2449–2474

Loomis TP (1972b) Diapiric emplacement of the Ronda high-temperature ultramafic intrusion, southern Spain. Geol Soc Am Bull 83: 2475–2496

Loomis TP (1972c) Coexisting aluminum silicate phases in contact metamorphic aureoles. Am J Sci 272: 933–945

Loomis TP (1975a) Tertiary mantle diapirism, orogeny and plate tectonics east of the Strait of Gibraltar. Am J Sci 275: 1–30

Loomis TP (1975b) Reaction of zoning of garnet. Contrib Mineral Petrol 52: 285–305

Loomis TP (1976) Irreversible reactions in high-grade metapelitic rocks. J Petrol 17: 559–588

Loomis TP (1977) Kinetics of a garnet granulite reaction. Contrib Mineral Petrol 62: 1–22

Loomis TP (1979) A natural example of metastable reactions involving garnet and sillimanite. J Petrol 20: 271–292

Lundeen MT (1978) Emplacement of the Ronda peridotite, Sierra Bermeja, Spain. Geol Soc Am Bull 89: 172–180

McPhail DC, Berman RG, Greenwood HJ (1990) Experimental and theoretical constraints on aluminum substitution in magnesian chlorite, and a thermodynamic model for H_2O in magnesian cordierite. Can Mineral 28: 859–874

Monié P, Galindo-Zaldívar J, González-Lodeiro F, Goffé B, Javaloy A (1991) $^{40}Ar/^{39}Ar$ geochronology of Alpine tectonism in the Betic Cordilleras (southern Spain). J Geol Soc London 148: 288–297

Monié P, Torres-Roldán RL, García-Casco A (1994) Cooling and exhumation of the western Betic Cordilleras, $^{40}Ar/^{39}Ar$ thermochronological constraints on a collapsed terrane. Tectonophysics 238: 353–379

Myers J, Eugster HP (1983) The system Fe-Si-O: oxygen buffer calibration to 1500 K. Contrib Mineral Petrol 82: 75–90

Pattison DRM (1989) *P-T* conditions and the influence of graphite on pelitic phase relations in the Ballachulish aureole, Scotland. J Petrol 30: 1219–1244

Pattison DRM (1994) Are reversed Fe-Mg exchange and solid solution experiments really reversed? Am Mineral 79: 938–950

Pattison DRM, Harte B (1991) Petrography and mineral chemistry of pelites. In: Voll G, Topel J, Pattison DRM, Seifert F (eds) Equilibrium and kinetics in contact metamorphism: the Ballachulish igneous complex and its aureole. Springer Verlag, Berlin Heidelberg New York Tokyo, pp 135–180

Pattison DRM, Tracy RJ (1991) Phase equilibria and thermobarometry of metapelites. In: Kerrick D.M. (ed) Contact metamorphism (Reviews in Mineralogy, 26) Mineral Soc Am, Washington, DC, pp 105–206

Pattison DRM, Spear FS, Cheney JT (1996) Are metamorphic muscovite + cordierite + staurolite + biotite assemblages stable or metastable? Implications for low pressure metapelitic phase equilibria (abstract). Geol Assoc Can Annu Meet Abstr Program 21: A73

Platt JP, Vissers RLM (1989) Extensional collapse of thickened continental lithosphere: a working hypothesis for the Alboran Sea and Gibraltar Arc. Geology 17: 540–543

Platt JP, Soto JI, Comas MC (1996) Decompression and high-temperature-low-pressure metamorphism in the exhumed floor of an extensional basin, Alboran Sea, western Mediterranean. Geology 24: 447–540

Platt JP, Soto JI, Whitehouse MJ, Hurford AJ, Kelley SP (1998) Thermal evolution, rate of exhumation, and tectonic significance of metamorphic rocks from the floor of the Alboran Extensional Basin, western Mediterranean. Tectonics 17: 671–689

Powell R, Holland T (1990) Calculated mineral equilibria in the pelite system, KFMASH (K_2O-FeO-MgO-Al_2O_3-SiO_2-H_2O). Am Mineral 75: 367–380

Pownceby MI, Wall VJ, O'Neill HStC (1987) FeMn partitioning between garnet and ilmenite: experimental calibration and applications. Contrib Mineral Petrol 97: 116–126

Pownceby MI, Wall VJ, O'Neill HStC (1991) An experimental study of the effect of Ca upon garnet-ilmenite Fe-Mn exchange equilibria. Am Mineral 76: 1580–1588

Reinhardt J, Kleemann U (1994) Extensional unroofing of granulitic lower crust and related low-pressure, high-temperature metamorphism in the Saxonian granulite massif, Germany. Tectonophysics 238: 71–94

Robie RA, Hemingway BS, Fisher JR (1978) Thermodynamic properties of minerals and related substances at 298.15 K and 1 bar (105 pascals) pressure and at higher temperatures. US Geol Surv Bull 1452

Ryzhenko BN, Volkov VP (1971) Fugacity coefficients of some gases in a broad range of temperatures and pressures (English translation). Geokhimiya 7: 760–773. In Russian (1971) Geochem Int. 8: 468–481

Sánchez-Rodríguez L, Gebauer D, Tubía JM, Gil Ibarguchi JI, Rubatto D (1996) First shrimp-ages on pyroxenites, eclogites and granites of the Ronda complex and its country rocks. Geogaceta 20: 487–488

Sanz de Galdeano C (1989) Estructura de las Sierras de Tejeda y de Cómpeta (Conjunto Alpujárride, Cordilleras Béticas). Rev Soc Geol Esp 2: 77–84

Skippen GB, Gunter AE (1996) The thermodynamic properties of H_2O in magnesium and iron cordierite. Contrib Mineral Petrol 124: 82–89

Sosson M, Morillon AC, Bourgois J, Féraud G, Poupeau G, Saint-Marc P (1998) Late exhumation stages of the Alpujarride complex (western Betic Cordilleras, Spain): new thermochronological and structural data on Los Reales and Ojen nappes. Tectonophysics 285: 253–273

Soto JI, Platt JP (1999) Petrological and structural evolution of high-grade metamorphic rocks from the floor of the Alboran Sea Basin, Western Mediterranean. J Petrol 40: 21–60

Spear FS (1991) On the interpretation of peak metamorphic temperatures in light of garnet diffusion during cooling. J Metamorphic Geol 9: 379–388

Spear FS, Cheney JT (1989) A petrogenetic grid for pelitic schists in the system SiO_2-Al_2O_3-FeO-MgO-K_2O-H_2O. Contrib Mineral Petrol 101: 149–164

Spear FS, Menard T (1989) Program GIBBS: a generalized Gibbs method algorithm. Am Mineral 74: 942–943

Spear FS, Ferry JM, Rumble DIII (1982) Analytical formulation of phase equilibria: the Gibbs' method. In: Ferry J.M. (ed) Characterization of metamorphism through mineral equilibria (Reviews in mineralogy, 10) Mineral Soc Am, Washington, DC, pp 105–152

Symmes GH, Ferry JM (1992) The effect of whole-rock MnO content on the stability of garnet in pelitic schists during metamorphism. J Metamorphic Geol 10: 221–237

Thompson AB (1976a) Mineral reactions in pelitic rocks. I. Prediction of *P-T-X*(Fe-Mg) phase relations. Am J Sci 276: 401–424

Thompson AB (1976b) Mineral reactions in pelitic rocks. II. Calculation of some *P-T-X*(Fe-Mg) phase relations. Am J Sci 276: 425–454

Torres-Roldán RL (1974) El metamorfísmo progresivo y la evolución de la serie de facies en las metapelitas alpujárrides al S.E. de Sierra Almijara (Sector central de las cordilleras Béticas, S. de España). Cuad Geol 5: 21–77

Torres-Roldán RL (1979) The tectonic subdivision of the Betic zone (Betic Cordilleras, southern Spain): its significance and one possible geotectonic scenario for the westernmost Alpine belt. Am J Sci 279: 19–51

Torres-Roldán RL (1981) Plurifacial metamorphic evolution of the Sierra Bermeja peridotite aureole (southern Spain). Estud Geol 37: 115–133

Torres-Roldán RL, García-Casco A, García-Sánchez PA (1999) CSpace: an integrated workplace for the graphical and algebraic analysis of phase assemblages on 32-bit Wintel platforms. Comput Geosci (in press)

Tubia JM (1994) The Ronda peridotites (Los Reales nappe): an example of the relationships between lithospheric thickening by oblique tectonics and late extensional deformation within the Betic Cordillera (Spain). Tectonophysics 238: 381–398

Tubía JM, Cuevas J (1986) High temperature emplacement of the Los Reales peridotite nappe (Betic Cordillera, Spain). J Struct Geol 8: 473–482

Tubía JM, Gil-Ibarguchi I (1991) Eclogites of the Ojén nappe: a record of subduction in the Alpujárride complex (Betic Cordilleras, southern Spain). J Geol Soc London 148: 801–804

Tubía JM, Cuevas J, Gil Ibarguchi JI (1997) Sequential development of the metamorphic aureole beneath the Ronda peridotites and its bearing on the tectonic evolution of the Betic Cordillera. Tectonophysics 279: 227–252

Van der Wal D, Vissers M (1993) Uplift and emplacement of upper mantle rocks in the western Mediterranean. Geology 21:1119–1122

Van der Wal D, Vissers M (1996) Structural petrology of the Ronda peridotite, SW Spain: Deformation history. J Petrol 37: 23–43

Vissers RLM, Platt JP, Van der Wal D (1995) Late orogenic extension of the Betic Cordillera and the Alboran Domain: a lithospheric view. Tectonics 14: 786–803

Wang P, Spear FS (1991) A field and theoretical analysis of garnet + chorite + chloritoid + biotite assemblages from the tri-state (MA, CT, NY) area, USA. Contrib Mineral Petrol 106: 217–235

Westerhof AB (1977) On the contact relations of high-temperature peridotites in the Serranía de Ronda, southern Spain. Tectonophysics 39: 579–591

Xu G, Will T, Powell R (1994) A calculated petrogenetic grid for the KFMASH system with particular reference to contact metamorphosed pelites. J Metamorphic Geol 12: 99–119

Zeck HP (1996) Betic-Rif orogeny: subduction of Mesozoic Tethys lithosphere under eastward drifting Iberia, slab detachment shortly before 22 Ma, and subsequent uplift and extensional tectonics. Tectonophysics 254: 1–16

Zeck HP, Hansen BT, Torres-Roldán RL, García-Casco A, Martín-Algarra A (1989) A 21 ± 2 Ma age for the termination of the ductile alpine deformation in the internal zone of the Betic Cordilleras, South Spain. Tectonophysics 169: 215–220

Zeck HP, Monié P, Villa I, Hansen BT (1992) Very high rates of cooling and uplift in the Alpine belt of the Betic Cordilleras, southern Spain. Geology 20: 79–82